J. Fluid Mech. (1986), *vol.* 171, *pp.* 407–439
Printed in Great Britain

An experimental study of the upwelling response of stratified reservoirs to surface shear stress

By STEPHEN MONISMITH

Hydraulic Engineering Laboratory, Department of Civil Engineering,
University of California, Berkeley, CA 94720, USA†

(Received 21 May 1985 and in revised form 8 January 1986)

An experimental study of the dynamic response of non-rotating, stratified reservoirs to the application of surface shear stresses is presented. The experiments were made using two-layered and linear stratifications; a moving belt was used to supply a shear stress to the fluid. Detailed measurements of the density field show that upwelling occurs at all values of the Wedderburn number, W, rather than only occurring when $W < 1$. Differences between the two-layer theory and the present observations are attributed to the fact that the experimental stratifications were continuous, rather than layered. Shearflow dispersion is observed to be an important mechanism for distributing the effects of localized upwelling over the entire length of the mixed layer. A model of mixed-layer deepening based on upwelling and shearflow dispersion is presented and is compared to the observations of this and other experimental studies.

1. Introduction

Wind plays a major role in determining the thermal structure of many reservoirs and lakes. The energy imparted by the wind to the water column can result in both turbulent mixing of the temperature field with the concomitant redistribution of any surface heat fluxes, and in baroclinic motions which temporarily distort the temperature field. The purpose of this paper is to report an experimental study of the interaction of mixing and motions, particularly the way in which mixing results from motions associated with upwelling. This information can then be used to decide under what circumstances one-dimensional models of mixed-layer dynamics (e.g. Stefan & Ford 1975; Spigel, Imberger & Rayner 1985) might be applicable. Because upwelling mainly represents the attempt of the lake to balance the surface shear stress through the creation of horizontal pressure gradients associated with sloping isopycnals, the dynamic aspects of the response, rather than the mixing *per se*, will be the focus of the discussion which follows.

Analytical theories (Heaps & Ramsbottom 1966; Monismith 1985) of the inviscid response of an n-layered lake or reservoir to a wind stress having the form:

$$\tau(t) = \rho u_*^2 H(t), \tag{1}$$

where u_*^2 is the kinematic shear stress measured in the water, and $H(t)$ is the Heaviside step function, show that the response consists of a steady state solution characterized by tilting of the free surface and some or all n interfaces, and of a set

† Present address: Centre for Water Research, University of Western Australia, Nedlands, WA 6009, Australia.

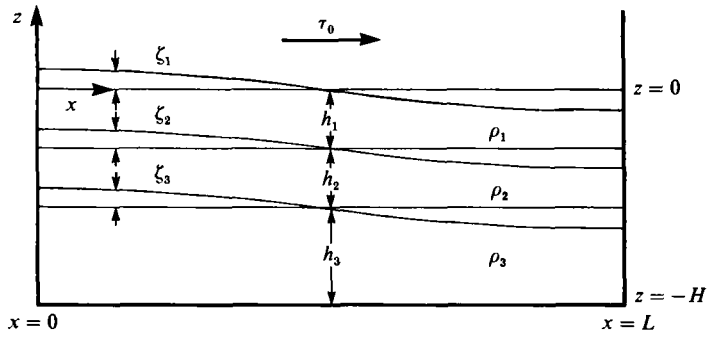

FIGURE 1. Definition sketch for the model n-layered reservoir. The case $n = 3$ is shown.

of n periodic deflections (seiches) of some or all n interfaces. The assumption that the shear stress vanishes below the interface closest to the free surface leads to the simple result, valid for all n, that only the free surface and internal interface closest to the free surface are tilted at steady state (Monismith 1985). Referring to figure 1, where the case $n = 3$ is shown, the slope of the first internal interface is found to be (Hellström 1941; Monismith 1985)

$$\frac{\partial \zeta_2}{\partial x} = -\frac{u_*^2}{\epsilon_{12} g h_1}, \tag{2}$$

where $\epsilon_{12} = (\rho_1 - \rho_2)/\rho_0$ and ρ_0 is the average density of the water column. Wu (1977) presents experimental evidence confirming (2).

Most of these analyses of the unsteady response have used $n = 2$ (Wedderburn 1912; Heaps & Ramsbottom 1966; Spigel & Imberger 1980); these give only one fundamental internal seiche mode, having a period

$$T_1 = \frac{2L}{\epsilon_{12} g h_1 h_2 / H}. \tag{3}$$

In this mode of motion, the two layers move in opposition, creating shear between the two layers. Seiches having periods T_1/m, where m is an arbitrary integer, are also possible, but usually the response is dominated by motions having the fundamental period T_1. In general, an n-layered lake will possess $(n-1)$ baroclinic modes having different vertical structure and periods (Lighthill 1969).

Spigel & Imberger (1980; hereinafter referred to as SI), were the first to combine a dynamical model of the response with a one-dimensional model of mixed-layer deepening. Using an integral energy model of mixed-layer dynamics and the case $n = 2$, they showed that the strength of the interaction between mixing and motions is determined by the relative importance of the two sources of turbulent kinetic energy (TKE) and depends on the Richardson number

$$Ri = \frac{\epsilon_{12} g h_1}{u_*^2}, \tag{4}$$

and the aspect ratio $A = L/h_1$. Their results are best summarized in terms of a combined parameter, the Wedderburn number (Thompson & Imberger 1980), defined as

$$W = Ri\, A^{-1}. \tag{5}$$

Simply put, the Wedderburn number is the seiche/set-up amplitude (for $n = 2$) non-dimensionalized by the mixed-layer depth; i.e. it is the usual measure of nonlinearity of long internal waves.

According to SI, when $W > 1$, the seiche response is unaffected by mixed-layer deepening which is predominantly by means of stirring of the surface layer (Kraus & Turner 1967; Wu 1973). If $W < 1$, the unsteady interfacial shear contributes significantly to the mixing process; for sufficiently small W, shear mixing (Pollard, Rhines & Thompson 1973) and Kelvin–Helmholtz billowing are the dominant processes. In this case, the seiche can be overdamped by mixing of momentum between the two layers. Kranenburg's (1984) laboratory experiments at $W \ll 1$ show excellent agreement between measured rates of mixed-layer deepening and those predicted by SI. However, as noted by SI, the mixed-layer depth can be expected to vary considerably over the length of the reservoir when $W \sim 1$, since according to (2), interfacial displacements $O(h_1 W^{-1}) \sim h_1$ are expected to occur. At the very least, Ri, and hence entrainment rates, should vary considerably along the length of the reservoir (Kranenberg 1985). Thus the one-dimensional model of mixed-layer dynamics may not be entirely accurate.

Imberger (1985) presents field observations of the dynamics of the mixed layer in Wellington Dam, Western Australia which confirm SI's analysis. It should be noted that while Imberger (1985) used SI's two-layer results, the measured stratification was far from two-layered. W was defined using the difference in density between the mixed-layer and the fluid immediately beneath, and the mixed-layer depth. If W had been based on the total charge in density over the entire water column and upon the depth of the seasonal thermocline (which possessed the largest density jump), i.e. upon a two-layer representation of the whole density profile, it would have been several orders of magnitude larger.

Thus, if g' and h_1 can be correctly chosen, SI's theory provides a useful model of one-dimensional deepening processes in stratified reservoirs. It is apparently applicable for $W \ll 1$ and $W \gg 1$, since in both cases the mixed-layer base remains horizontal. Two questions remain: What happens when $W \approx 1$ and how are appropriate values of g' and h_1 to be chosen? More importantly, where the interface actually surfaces, or, equivalently, the lower layer upwells, a different mixing mechanism, one which is entirely two-dimensional might be observed.

Keulegan & Brame (1960) described such a mechanism, later termed 'edge leakage' by Blanton (1973). The situation at the upwelling front is sketched in figure 2. Upwelled fluid is incorporated into the near-surface drift and flows over lighter surface waters, leading to density inversions and thus to turbulence and mixing. Keulegan & Brame's (1960) laboratory results show horizontal density gradients in the mixed layer at all values of W in the range $0.35 < W < 10$, implying some form of upwelling can occur for $W > 1$. Thompson & Imberger's (1980) (also Church & Thompson 1982) numerical simulations also showed signs of upwelling at $W = 4$.

This experimental and numerical evidence of upwelling at $W > 1$ cannot be explained within the framework of the two-layer theory; however, it can be easily explained through the use of a simple, heuristic argument, based on the n-layer case. Any real stratification will be continuous or at least layered on a scale much less than the total depth of the reservoir (e.g. as reported in Imberger 1985), hence the number of layers required to accurately model the stratification should be quite large. Thus the density jump ϵ_{12} will be much less than the total vertical density contrast and in like fashion, h_1 will be much less than H. Upwelling of fluid from the second layer will then take place for wind streses much weaker than those required to produce

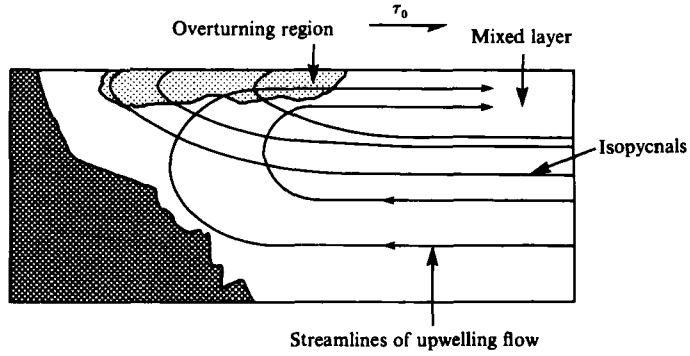

FIGURE 2. Sketch of upwelling region showing 'edge leakage' (after Blanton 1973).

upwelling in a two-layered representation of the stratification. Furthermore, if the stratification is truly continuous, n should be infinite. However, as the number of layers used to represent the stratification is made larger, the density difference ϵ_{12} becomes smaller, as does W. Clearly n could be chosen such that $W = 1$.

This simple argument can be rephrased into a more useful form as follows. If W is defined using overall parameters such as the distance from the free surface to the seasonal thermocline and the total density change from the water surface to the bottom of the reservoir, then fluid that is very close to the mixed-layer base will upwell when $W \gg 1$, while bottom fluid will upwell when $W < 1$. The former will be termed partial upwelling while the latter will be referred to as total upwelling. Total upwelling is commonly associated with the fall overturn in lakes (Mortimer 1952; Stefan & Ford 1975). The analysis of the response of a continuously-stratified reservoir reported in Monismith (1986) shows that this heuristic argument is correct subject to the crucial assumption that the shear stress drops to zero at the base of the mixed layer. The justification for this assumption is that the stratification below the mixed layer supresses horizontal as well as vertical motions below the mixed layer at steady state via endwall blocking (see Turner 1973, pp. 79 ff). This means that the stress must be zero where the density gradient is not zero.

In order to test these conclusions concerning the occurrence of upwelling when $W > 1$, and to examine the nature of upwelling and its effect on mixing when W defined using bulk parameters is $O(1)$, a series of laboratory experiments was performed. Rather than use wind stress, a belt was used to supply shear stress to fluid contained in a box and stratified either as two layers separated by a finite-thickness interface, or with a linear variation of density with height. The experimental apparatus and procedures are described in §2. The experimental results are described in §3. Results concerning shear-flow dispersion and mixed-layer deepening are presented in §4. Conclusions are presented in §5. Lastly, a simple model of mixed-layer deepening based entirely on upwelling is developed in the Appendix. Analysis of the data in terms of the normal-mode response (Lighthill 1969) when $W > 1$ forms the basis of a separate publication (Monismith 1986).

2. Experimental apparatus and procedures

The experiments were performed using a belt to simulate the wind stress. This offers two advantages over using wind: first, the boundary conditions on the stressed surface are known; second, the belt speed and direction are easily controlled. The

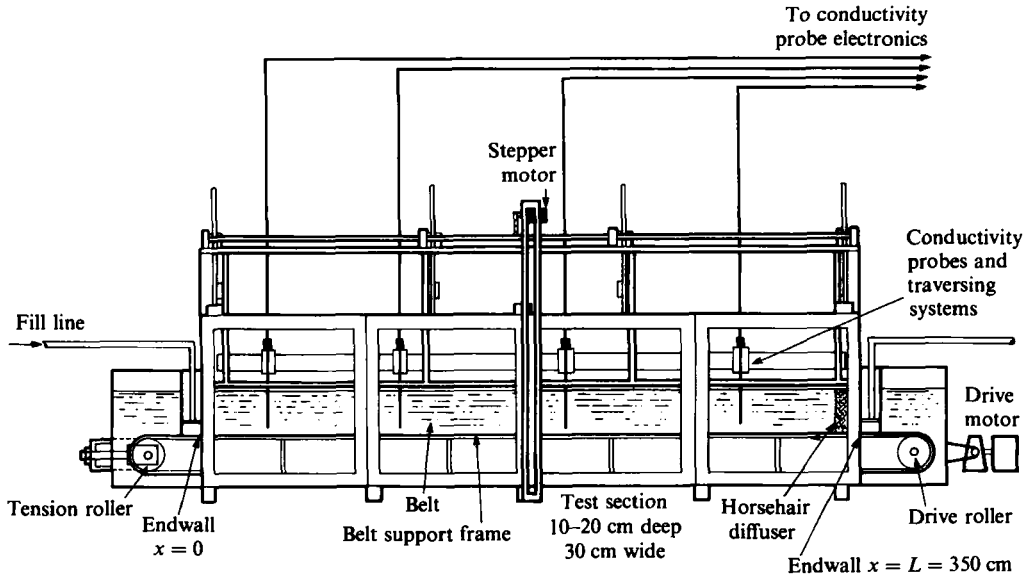

FIGURE 3. The experimental apparatus.

belt was mounted on the bottom of the tank rather than at the water surface to allow the conductivity probes to enter the fluid from above. Due to the presence of surface films, the free surface acted as a no-slip boundary.

Because of the small density differences used in the experiments, application of the stress at the bottom surface of the fluid rather than at the free surface should not significantly affect the results. In order to discuss the experimental results, it is however, necessary to redefine the term upwelling to mean a vertical flow downwards, i.e. towards the belt. Rather than the coordinate system shown in figure 1, the experimental coordinates will have z positive downwards, with the origin taken to be the free surface above the point where the belt enters the test section (which has coordinates $x = 0, z = H$). The term downwind thus means in the direction of increasing x while upwind means in the direction of decreasing x.

The experiments were performed in a rectangular tank 4.0 m long, 305 mm wide, and with fluid depths ranging from 100 to 200 mm above the belt. The tank, shown in figure 3(*a*) was divided into three sections: the test section (3.5 m long) and two Perspex boxes, one at each end of the test section. To eliminate extraneous mixing near the rollers, the test section was bounded on each end by double walls, allowing the belt to pass in and out of the test section while permitting only a small amount of fluid (approximately 1 ml s^{-1} at the highest belt speeds) to be exchanged between the test section and the rest of the tank. This amount of leakage was sufficient to limit the experiments to no more than about 2000 s. The belt was supported underneath by a steel frame, coated with Teflon to minimize friction and was driven by a d.c. motor. Estimates of the stress between the fluid and the belt showed that the torques associated with friction in the seals on the belt would be much greater than any torques due to stress on the fluid; therefore, no attempt was made to use torque to measure the applied shear stress directly.

Preliminary experiments showed that where the near-belt boundary layer was turned vertically by the endwall at $x = 3.50$ m, a narrow, intense jet formed. Mixing resulting from impingement of this jet on the interface appeared to be much more

vigorous than either mixing along the length of the interface, or mixing in the upwelling region (near $x = 0$). A similar flow pattern is clearly evident in Kosef & Street's (1985) experimental observations. This mixing mechanism was considered to be undesirable, as it appeared to be an effect of the geometry of the corner at $x = 3.5$ m, and not necessarily a mixing process which would be observed in nature. In order to suppress the jet, a 50 mm thick piece of rubberized horsehair was mounted on the test-section side of the endwall at $x = 3.50$ m.

Since salt was used to obtain density variations, the vertical distributions of density were obtained from periodic, vertical traverses of a set of 4 or 6 two-electrode conductivity probes (vertical resolution = 5 mm) mounted on a stepper-motor-driven rail extending the length of the tank. In general, a single profile took approximately 5 s to complete. The length of time between profiles was generally no more than $0.16\,T_1$ (15 s maximum); the conductivity measurements have quite good temporal resolution of the evolving density field. To avoid the effects of probe wakes, probe outputs were sampled only on downward traverses. A description of the design of the probes and associated circuitry (including multiplexers to eliminate groundloops) and the data acquisition system can be found in Monismith (1983).

The experiments were performed as follows. The tank was first stratified and then left for 1 to 2 hours to allow residual motions to die out before proceeding. After 4 profiles had been taken to establish the initial conditions, the motor was started, setting the belt in motion. In some experiments, photographs of a shadowgraph image of the central region were taken at regular intervals during the start-up phase. At a predetermined time the motor was stopped; profiling continued until the fluid came to rest. Once profiling was completed, the conductivity probes were calibrated, and the sampled voltages converted to densities.

A total of 25 experiments using two-layer and linear stratifications were performed. Tables 1 and 2 give experimetal data such as fluid depth, belt speed, and total density difference. Layer thicknesses for two-layered flows were calculated by assuming that the interface coincided with the point of the maximum density gradient. In all of what follows the term 'two-layer stratification' will refer to two homogeneous layers separated by a finite thickness interface (generally about 15% of the total depth). Because the stress was applied to the salt-water layer, h_2 was used in (5) to calculate W rather than using h_1. For experiments with linear stratifications, h_2 was set equal to $\frac{1}{2}H$ and $g' = \frac{1}{2}N^2H$. This provides a convenient basis for comparing those experiments conducted with two-layered stratifications with those performed with linear stratifications.

Calculation of W requires that the stress be known. The stresses reported in tables 1 and 2 were calculated from the experimental data as follows. For experiments with $W > 1$, at steady state the hydrostatic pressure gradient associated with the perturbation density field balances the shear stress gradient in the mixed layer. Thus the shear stress can be deduced from measurements of the perturbation density field. Assuming the pressure is hydrostatic, and neglecting sidewall stresses and advective and unsteady accelerations, it can be shown (see Monismith 1983 for details) that the mean shear stress, τ_0, applied to the fluid by the belt between x_1 and x_2 is found to be

$$\tau_0 = \left(\int_0^H \int_0^z (\rho'(x_2, \phi) - \rho'(x_1, \phi))\, g\, \mathrm{d}\phi\, \mathrm{d}z\right) \Big/ (x_2 - x_1). \tag{6}$$

where $\rho'(x_i, z)$ is the perturbation density at distance z below the free surface and distance x_i from the origin.

The accuracy of (6) depends on the size of errors introduced through neglect of

Experiment	h_2 cm	H cm	$\epsilon_{12}g$ cm s^{-2}	U_B cm s^{-1}	u_*^2 cm^2 s^{-2}	Ri	L/h_2	W	T_0 s
1*a*	10.0	20.0	14.2	11.0	0.34	418	35	11.9	622
1*b*	10.0	20.0	14.2	21.7	1.18	120	35	3.4	454
2	10.0	20.0	13.0	11.0	0.44	295	35	8.4	655
5	12.0	20.0	13.6	18.5	0.70	233	29	8.0	1713
6	13.0	20.0	12.0	18.5	1.20	130	27	4.8	655
7	10.0	20.0	13.2	14.0	0.50	264	35	7.5	2386
8	10.0	20.0	11.0	20.3	0.80	138	35	3.9	874
9	12.0	20.0	18.3	15.0	0.90	244	29	8.4	3930
10	13.0	20.0	15.0	15.0	0.80	244	27	9.0	2134
16	5.0	10.0	10.0	13.0	0.70	71	70	1.0	767
17	5.0	10.0	7.5	20.6	1.5	25	70	0.4	773
18	5.0	10.0	10.0	26.4	2.3	23	70	0.3	840
19	5.0	10.0	6.3	26.4	2.2	14	70	0.2	368
20	6.0	10.0	10.0	13.7	0.60	100	58	1.7	762
21	5.8	15.0	10.0	13.0	0.56	103	60	1.7	762
22	8.5	15.0	10.0	21.3	1.2	69	41	1.7	1188
23	5.0	10.0	10.0	25.6	2.0	25	70	0.4	147
24	5.0	10.0	10.0	22.5	1.6	31	70	0.4	1355
25	12.0	20.0	9.4	21.4	1.0	113	29	3.9	2100
33	3.0	7.0	9.4	11.5	0.6	47	116	0.4	448
34	3.7	12.0	9.4	5.9	0.25	139	95	1.5	835
35	4.0	8.0	7.8	20.3	1.2	26	88	0.3	960

TABLE 1. Experimental programme: two-layer stratifications

U_B is the belt speed; T_0 is the amount of time which the belt was run during a particular experiment; Horsehair diffuser not used in experiments 1*a* to 6; u_*^2 calculated using C_D in experiments where $W < 1$.

Experiment	H cm	h cm	N^2H cm s^{-2}	U_B cm s^{-1}	u_*^2 cm^2 s^{-2}	Ri	L/H	W	T_0 s
15	10.0	1.5	9.4	25.4	2.2	43	35.0	0.4	779
28	25.0	2.6	8.0	26.1	0.90	222	14.0	4.0	824
29	20.0	2.5	8.5	8.1	0.20	800	17.5	12.0	1033
30	20.0	5.0	6.1	14.0	0.70	173	17.5	2.5	1230
31	20.0	10.0	5.0	26.2	2.2	45	17.5	0.7	148
32	16.4	1.7	8.1	17.6	0.9	147	21.3	1.7	1143

TABLE 2. Experimental programme: linear stratifications

h is the thickness of the mixed layer adjacent to the belt at the start of the experiment; N^2 is the buoyancy frequency squared $= (g/\rho)(d\rho/dz)$; Ri is calculated using (4), substituting H for h_1; u_*^2 calculated using C_D in experiments 15 and 31.

various terms in the x-momentum equation when performing the integrations leading up to (6), and on errors in measurement of the perturbation density field. The calculated kinematic shear-stress gradient is $O(u_*^2/h_2)$. Advective accelerations are $O(u_*^2/L)$ (Keulegan & Brame 1960). Since they are $O(h_2/L)$ times as large as the shear-stress gradient, their neglect introduces an error of approximately 5% in the calculated stress. The total force developed by sidwall stresses can be estimated as $2C_W u_*^2 h_2 L$, where C_W is a drag coefficient that would be at most 0.025 (Schlichting 1975). Since the force applied by the belt to the fluid was $u_*^2 BL$, where B is the width

of the belt, the neglected sidewall stress would have been only $2C_W h_2/B \approx 0.02$ as large as the applied stress.

Equation (6) also assumes that the free surface is flat at steady state. Because the free-surface pressure gradient at steady state balances the small, laminar shear-stress gradient in the fluid above the mixed layer, this assumption leads to an error that is very much smaller than errors introduced by neglect of advective accelerations and sidewall stresses (Monismith 1983).

Errors in the calculated stress arise mainly from the accuracy with which the perturbation density field can be measured. It is shown in Monismith (1983) that errors in calibration and probe position lead to errors in calculating τ_0 that are roughly 20% of τ_0 itself. Both of these experimental errors were partially corrected for by noting any zero-offsets appearing in the stress histories. Hence, their combined effect would have been much less than estimated above.

The shear velocity was generally 5–6% of the belt velocity in the present experiments, consistent with the observation that in wind-driven flows the surface drift velocity is generally $20\,u_*$ (Fitzgerald & Mansfield 1965; Keulegan 1951). As (6) is not valid once full upwelling has taken place (the free-surface pressure gradient is no longer negligible), i.e. when $W < 1$, it was necessary in some cases to estimate the shear stress using a value of the drag coefficient estimated from measurements of the shear stress at similar mixed-layer Reynolds numbers ($U_B h_2/\nu$).

3. Experimental results

3.1. *Two-layer flows, $W > 2$*

According to the theory discussed in §1, the response of a two-layered fluid at $W > 1$ to an impulsively applied wind stress should consist of a decaying internal seiche and, in the absence of any two-dimensional effects, a slow deepening of the mixed layer by stirring. As observed, internal seiches were a prominent feature of the fluid response, both when the stress was applied and when it was removed. However, they were accompanied by considerable distortions of the interface, transient, jet-like flows in the interface, and partial upwelling.

The dynamic response is neatly summarized by the time history of the shear stress calculated using (6) which is shown as figure 4. Upon start-up of the belt, there is both a net force, directed towards $x = 0$, and a set of decaying oscillations at a period of approximately 100 s, which is the first-mode internal seiche period (T_1). When the belt is stopped, the net force drops to 0 and a new set of oscillations begin. Although the density field is strongly disturbed from its one-dimensional state, both the period and amplitude of these oscillations are in excellent agreement with both the two-layer theory and the normal-mode theory for continuously-stratified fluids (Monismith 1986).

Once the belt was set in motion, a boundary layer several millimetres thick developed adjacent to the belt. Visualization of the flow using dye streaks showed that the velocity of the fluid within the boundary layer varied between the belt speed and zero. After several seconds (as seen at $x = \frac{1}{2}L$) an opposing flow, nearly uniform with depth at a speed of approximately 3–5% that of the belt itself, developed outside the boundary layer. This flow is sketched in figure 5(*a*).

After approximately $\frac{1}{2}T_1$, the return flow became concentrated in the top of the mixed layer, as is sketched in figure 5(*b*). This flow appeared turbulent and always originated at the downwind wall ($x = 350$ cm). The concentrated return flow appeared to plunge as it flowed upwind, and was incorporated into the mixed layer within 20

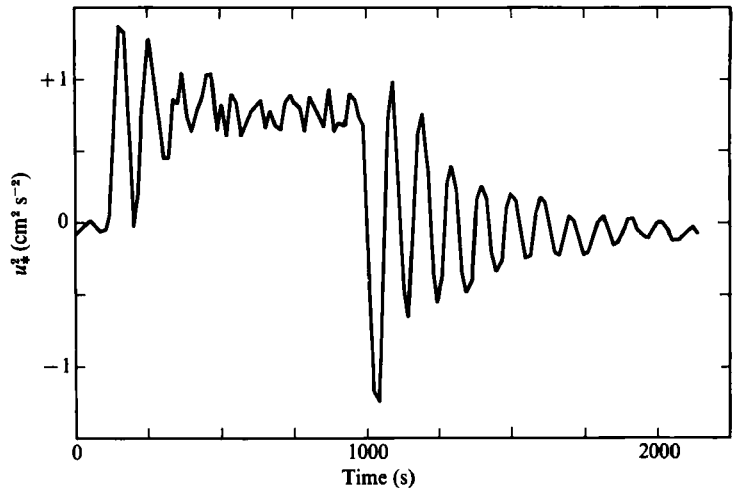

FIGURE 4. Time history of u_*^2 in experiment 8 ($W = 3.9$, two layers) calculated according to (6).

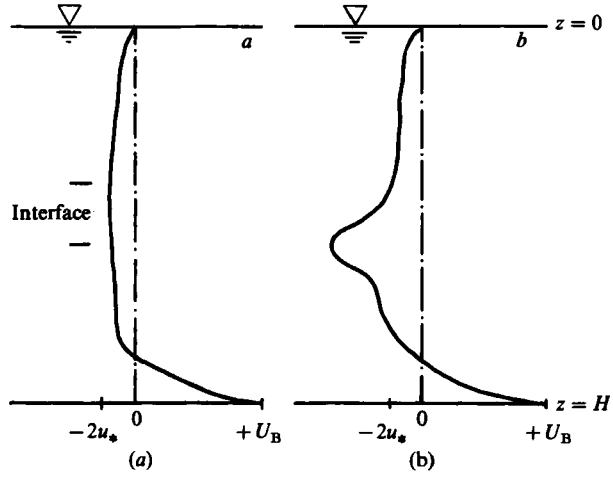

FIGURE 5. (*a*) Velocity profile when $t \ll T_1$ showing initial barotropic flow. (*b*) Velocity profile for $t > \frac{1}{4}T_1$ showing jet-like flow in the interface when $W > 1$.

or 30 cm of the upwind ($x = 0$) wall. The plunging of this flow can be attributed to the tilting of the isopycnals close to the mixed-layer base. Based on shadowgraph observations, an example of which is shown in figure 6, the interface always appeared to surface.

The effect of the concentrated return flow was to sharpen the interface at the downwind end and to diffuse it at the upwind end, as shown in measurements of the density field. Figure 7 (*a*)–(*d*) shows contour plots of the density field during the initial phase of experiment 8 ($W = 3.8$). Tilting of the interface by the internal seiche is evident in figure 7 (*a*) ($t = 0.32\,T_1$). Between $t = 0.32\,T_1$ and $0.96\,T_1$ the interface underwent a remarkable transformation: at $x = 300$ cm ($0.85\,L$): it decreased in thickness from 5 cm to less than 5 mm (filtering involved in producing the contour plot tends to obscure how sharp the interface was at the upwind end) while at $x = 32$ cm ($0.08\,L$) it expanded until it filled the lower two-thirds of the water

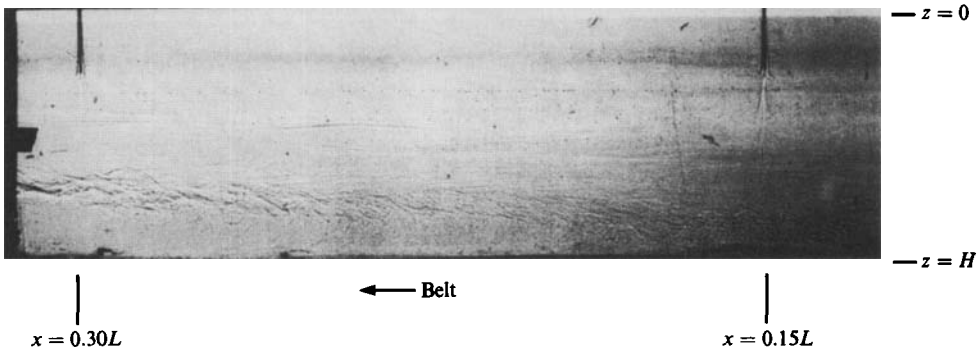

FIGURE 6. Shadowgraph of upwelling region for two-layer flow at $W > 1$. This photo shows the steady-state density field during experiment 5 ($W = 8$) in the region $0 < x < 0.25\,L$. The interface intersecting the belt near $x = 0$ has a density jump that is approximately 5% of the total density contrast between the layers.

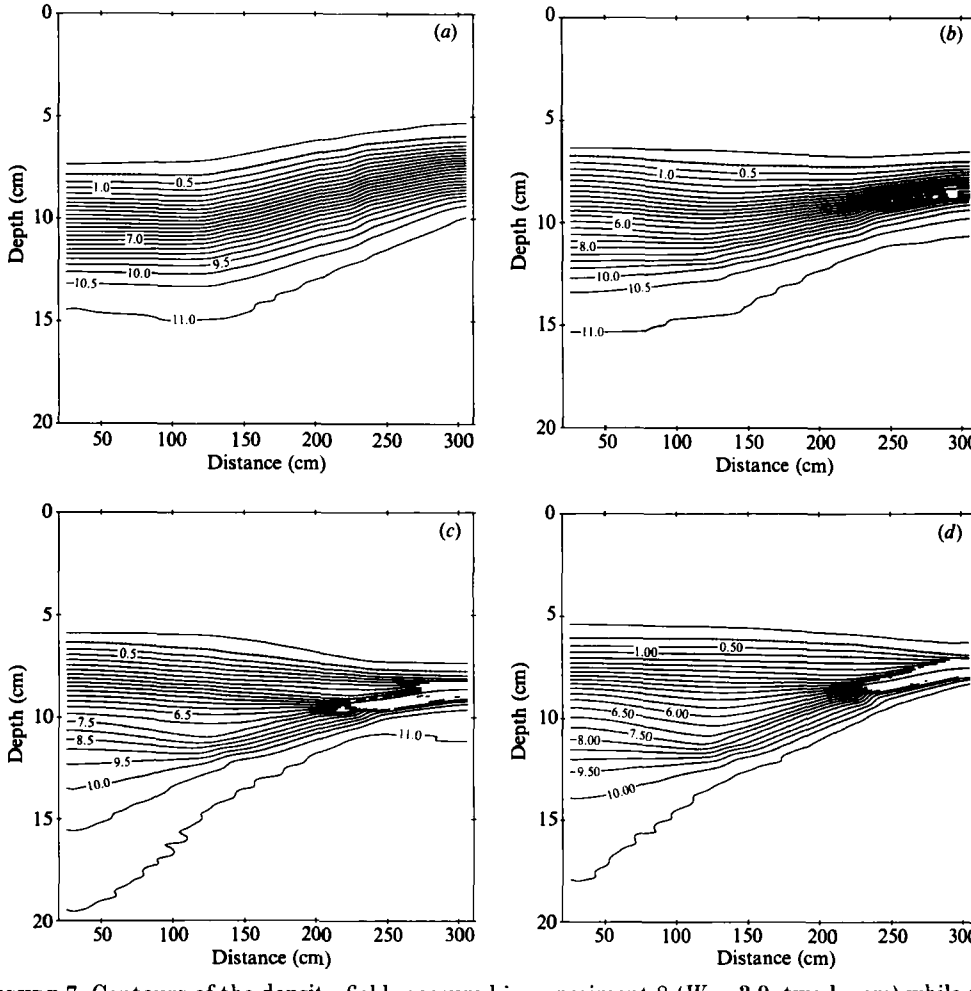

FIGURE 7. Contours of the density field measured in experiment 8 ($W = 3.9$, two layers) while the belt was running. The belt is on the bottom of the tank and moves from left to right. The times are as follows: (*a*) $0.32\,T_1'$, (*b*) $0.64\,T_1'$, (*c*) $0.96\,T_1'$, and (*d*) $8.0\,T_1'$.

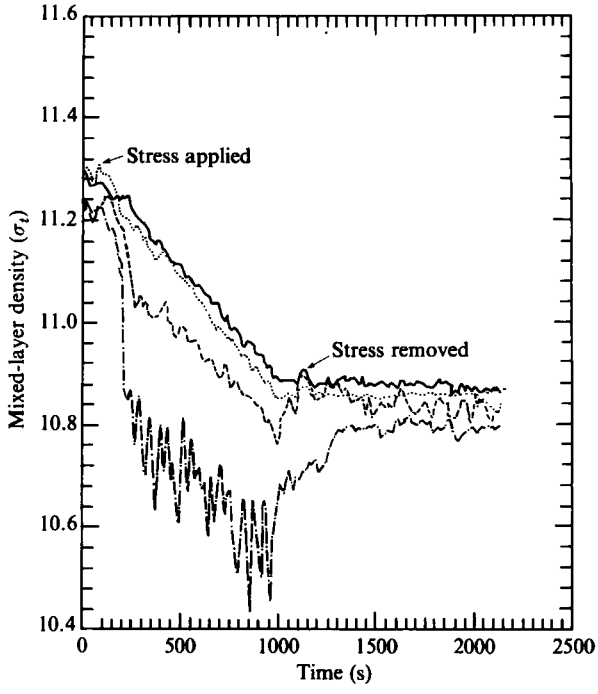

FIGURE 8. Mixed-layer density as a function of time during experiment 8 at —·—, $x = 0.08\,L$; – – –, $x = 0.37\,L$; · · · · · ·, $x = 0.66\,L$, and ——, $x = 0.88\,L$.

column. Plots of the density field at later times showed that the interface continued to sharpen (and diverge) until $t \approx 1.5\,T_1$.

Figure 7 (*d*) shows a picture of the density field at $t = 8.3\,T_1$; this may be taken to represent steady-state conditions, those conditions which vary on a timescale much longer than T_1, but are set-up in a time $O(T_1)$. None of the sets of profiles taken after $t \approx 1.5\,T_1$, differ very much from those making up figure 7 (*d*). The interface does not tilt bodily along the length of the tank; the depth of the $10.5\,\sigma_T$ contour (where σ_T is taken to mean $\rho - 1000$ [kg m^{-3}]), that contour line closest to the edge of the mixed layer, varies by 12 cm, while the $3\,\sigma_t$ contour is virtually flat. Hence the two-layer theory is inadequate as far as prediction of the steady-state density field is concerned. The fact that Wu (1977) was able to describe his observations using a two-layer theory is probably due to the fact that his experiments were performed with considerably sharper interfaces than those in the present study. Furthermore, Wu did not measure the density field directly in his experiments and therefore would not have detected the changes in interfacial thickness and density jump measured in the present experiments.

Although the density field appeared nearly two-dimensional, the velocity field at steady state was observed to be three-dimensional. Near the endwalls, velocities in the direction perpendicular to the sidewalls were comparable to velocities in the direction parallel to the sidewalls. Koseff & Street (1985) emphasize the three-dimensional nature of the velocity field in their stratified cavity-flow experiments.

The occurrence of upwelling is best illustrated in figure 8 which plots mixed-layer density for different values of x, as functions of time during experiment 8. Here mixed-layer density is defined as the average density of fluid that is located no more than 1 cm from the belt. In response to application of the stress, a horizontal density

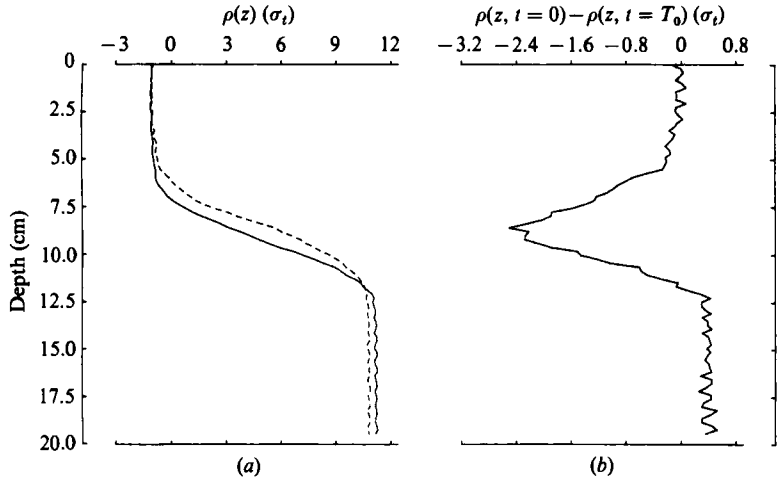

FIGURE 9. (*a*) Superposition of initial (——) and final (– – – –) density profiles in experiment 8. (*b*) Net density difference due to mixing, as a function of height for experiment 8.

gradient (averaging about 1.5×10^{-1} kg m^{-4}) is set up in the mixed layer. This gradient is maintained while the stress continues to be applied to the fluid, but disappears when the stress is removed. Most importantly, changes over time of mixed-layer density are independent of position; the mixed-layer density gradient is thus constant throughout the experiment. This gradient contributes significantly to the pressure gradient in the mixed layer, providing an average net force of roughly 1.5×10^{-4} N m^{-1} (based on an average mixed-layer depth of 10 cm) out of the total of 8×10^{-4} N m^{-1} provided by the perturbation density field.

When the belt was stopped, both a decaying seiche and, once again, an interfacial jet were observed as the fluid returned to a state of horizontal homogeneity. Further details of the unsteady response, both to application and removal of the stress can be found in Monismith (1986).

The net effect of having applied a stress to the fluid for a finite length of time (931 s), can be seen in figure 9(*a*) and (*b*) which show firstly a superposition of the initial and final profiles and secondly, the net change in the density profile, derived from figure 9(*a*), plotted as a function of height. The latter represents the effective, time-averaged, vertical buoyancy flux. In contrast to observations made in one-dimensional entrainment experiments (Linden 1979; Fernando & Long 1983), a comparison of the initial and final profiles fails to show any sharpening of the interface; the effective buoyancy flux does not, as is commonly assumed in one-dimensional mixing models, vanish above (below) the mixed-layer base.

3.2. *Two-layers*, $1 < W < 2$

When $1 < W < 2$, the initial seiche was overdamped. This is shown in figure 10, the stress time series for experiment 22 ($W = 1.7, h_1 = h_2$). For this range of W the interface was observed to tilt until it nearly reached the belt (according to linear, two-layer theory when $W = 1$, the interface just reaches the stressed surface at $t = \frac{1}{4}T_1$) near $x = 0$ and then to rebound to its equilibrium position. Figure 11 is a contour plot of the steady-state density field in experiment 22. The interface is sharp over most of the length of the tank; only for $x \leqslant 0.2\,L$ does the interface begin to diverge. It seems plausible that decreasing W has the effect of suppressing interfacial

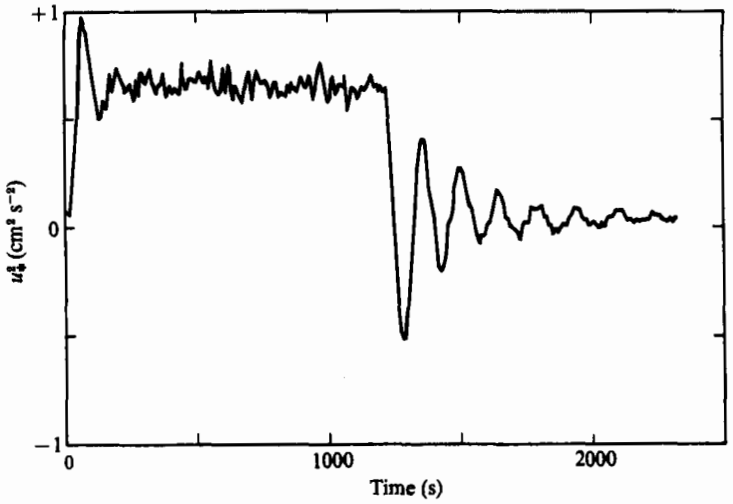

FIGURE 10. Time history of u_*^2 in experiment 22 ($W = 1.7$, two layers) calculated according to (6).

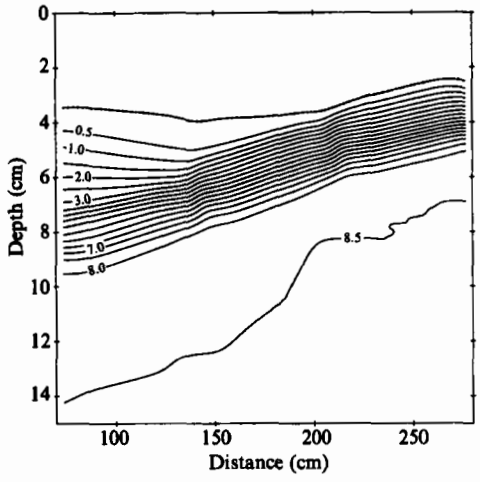

FIGURE 11. Contour plot of the steady-state density field measured in experiment 22.

divergence (see Monismith 1986 for further discussion of this point in connection with application of normal-mode theory to the present set of observations). Time series of the mixed-layer density for experiments in this range of W were remarkably similar to those measured at higher W and will not be shown here.

3.3. *Linear stratification, $W > 1$*

There was one major difference between experiments with linear stratifications and those with two-layer stratifications: in the experiments with linear stratifications, there was always substantial mixing associated with the initial mixed-layer formation. In fact the value of W calculated using mixed layer properties must be identically zero (ideally) if the stratification is linear, as both $g' = 0$ (no density jump) and $h_1 = 0$ (no mixed layer). However, as mentioned in §2, W was calculated using $h_1 = \frac{1}{2}H$ and $g' = \frac{1}{2}N^2H$.

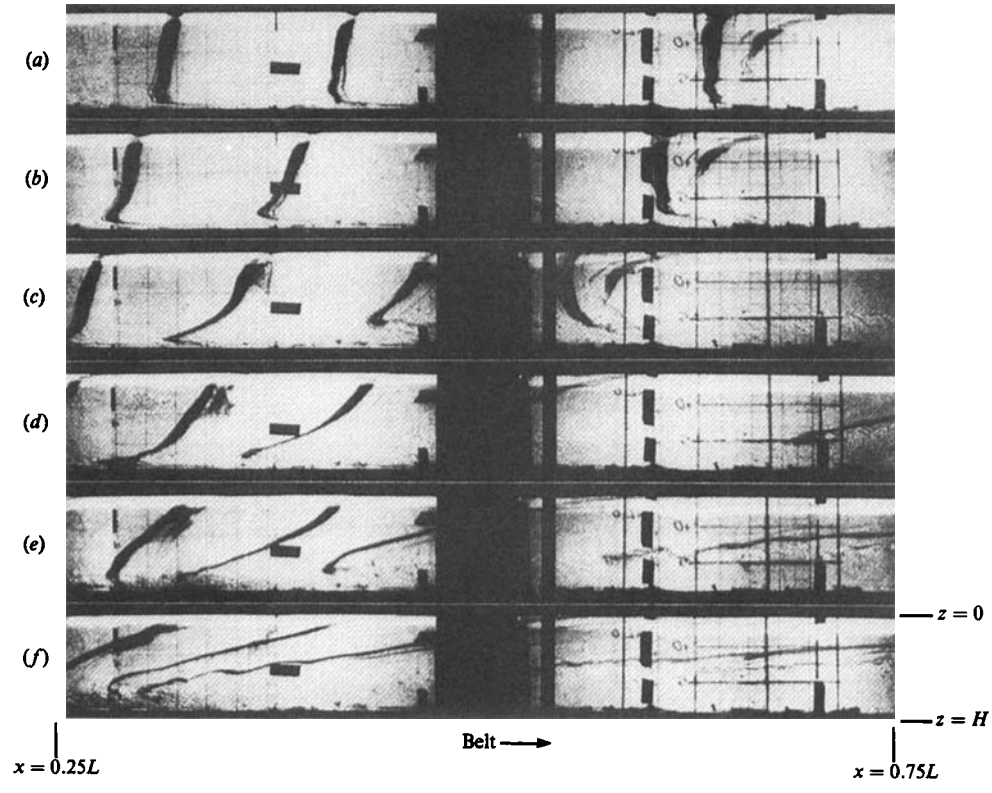

FIGURE 12. Shadowgraphs of the centre half ($0.25\,L > x < 0.75\,L$) of the test section during the initial phase of experiment 32 ($W = 1.7$, linear). The times are as follows: (*a*) $t = 0.08\,T_1$; (*b*) $t = 0.13\,T_1$; (*c*) $t = 0.18\,T_1$; (*d*) $t = 0.24\,T_1$; (*e*) $t = 0.29\,T_1$; and (*f*) $t = 0.34\,T_1$. The dye streaks show the intense jet that developed above the mixed layer.

Figure 12(*a*)–(*f*) shows a series of shadowgraphs which include dyestreaks indicating the velocity profiles at various instants during the start-up phase of experiment 32 ($W = 1.7$). Immediately after the belt was set in motion, the flow appeared barotropic. As in the two-layer case, a concentrated flow then developed rapidly above the mixed layer, giving the impression that flow above the mixed layer was directed towards an imaginary sink located on the belt near $x = 0$.

Density measurements made in experiment 32 will be used to demonstrate the evolution of the density field when the stratification is linear. Figure 13(*a*) ($t = 0.3\,T_1$, where $T_1 = 2L/(NH/\pi)$) shows the initial development of the mixed layer. It is apparent from this plot that the initial tilting of the interface (and other isopycnals as well) was quite asymmetric: vertical displacements of the isopycnals outside the mixed layer were 2 or 3 cm at mid-depth for $x > \frac{1}{2}L$ while they were less than 1 cm for $x < \frac{1}{2}L$.

By $t = 0.5\,T_1$ (figure 13*b*), the mixed-layer depth varied between 0 and 10 cm along the length of the tank, giving an average depth of approximtely 5 cm at that time. Figure 13(*c*) ($t = 1.0\,T_1$) shows that as upwelling proceeded, the average mixed-layer depth continued to increase while, at the same time, the fan-like structure of the density field observed in two-layer flows began to emerge. Figure 13(*d*) ($t = 6.1\,T_1$) shows the structure of the quasi-steady-state density field in experiment 32. Its most striking feature is the flatness of isopycnals outside the mixed layer and interface,

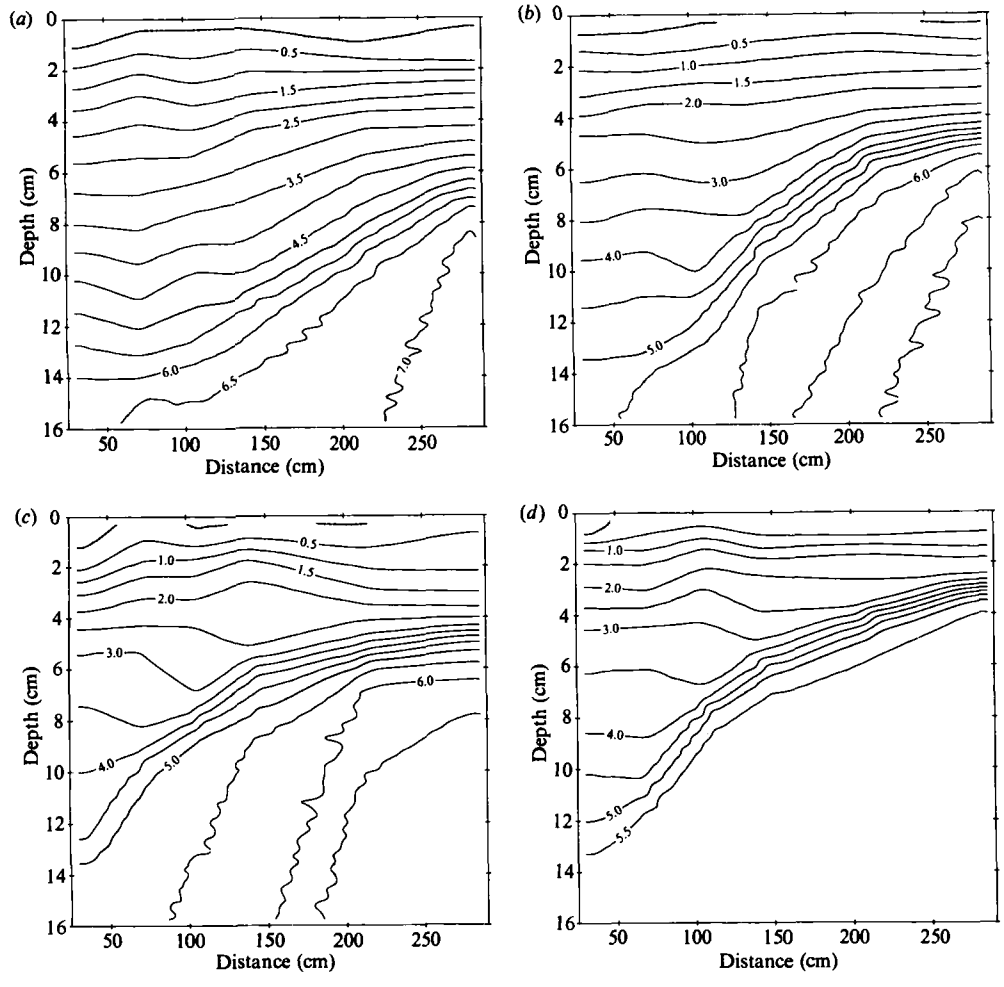

FIGURE 13. Contours of the density field measured in experiment 32 while the belt was running. The times are as follows: (*a*) $0.3\,T_1$; (*b*) $0.5\,T_1$; (*c*) $1.0\,T_1$; and (*d*) $6.1\,T_1$.

indicating the fluid above the mixed layer must have been nearly at rest, since the lack of isopycnal tilt also implies a lack of pressure gradient.

Figure 14 (*a*)–(*d*) shows complete sets of profiles of the quasi-steady-state density field for the following four experiments with linear stratifications: experiment 29 ($W = 12$), experiment 28 ($W = 4$), experiment 30 ($W = 2.5$), experiment 32 ($W = 1.7$). These profiles represent the condition of the density field after initial upwelling and mixing were complete, but before weak, sustained upwelling (as seen in figure 8) and other means of mixed-layer deepening had sensibly modified the density field. The similarity of the 4 sets of profiles is striking. For the sake of comparison, a Wedderburn number, W_a based on the average interfacial density jump, $\langle \Delta\rho \rangle$, and average mixed-layer depth, $\langle h \rangle$ was computed (using (5)) for each of these experiments. The results of this computation are presented in table 3.

All four experiments give values of W_a very nearly equal to 1. In each of the experiments, initial deepening was rapid until the average mixed-layer depths were approximately those recorded in table 2. The observed values of $\langle h \rangle / H$ can be easily

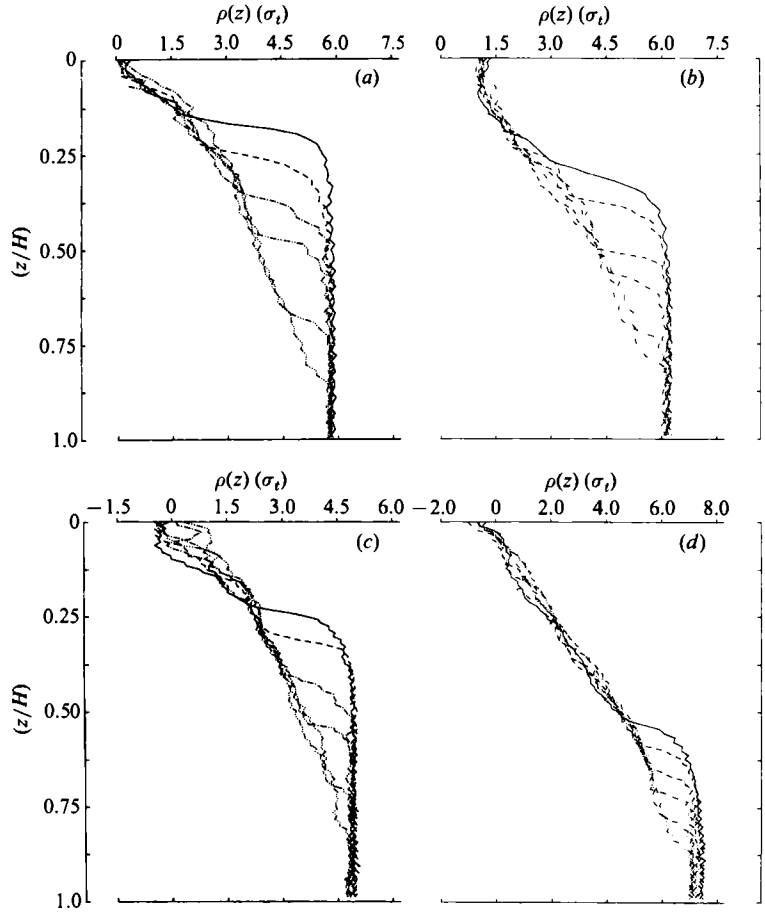

FIGURE 14. (*a*) Density profiles at steady state: experiment 29 ($W = 12$). The profiles were taken at —·····—, $x = 0.1\,L$; —···—, $x = 0.2\,L$; —··—, $x = 0.3\,L$; —·—, $x = 0.4\,L$; – – – –, $x = 0.6\,L$; and ——, $x = 0.8\,L$. The symbols have the same meaning in (*b*) to (*d*). (*b*) Density profiles at steady state: experiment 28 ($W = 4$). (*c*) Density profiles at steady state: experiment 30 ($W = 2$). (*d*) Density profiles at steady state: experiment 32 ($W_B = 1.7$).

accounted for as follows: if a one-dimensional mixed layer of depth h were to form in an initially linearly stratified fluid, $g' = \frac{1}{2}N^2h$; thus $W_a = N^2h^3/(2u_*^2 L)$. Setting this equal to 1 gives

$$\frac{h}{H} = (2W)^{-\frac{1}{3}}. \tag{7}$$

Predictions of the mixed-layer depth made using (7), are also shown in table 3; they agree with the observed average depths. Thus, in a linearly-stratified fluid, the mixed layer deepens rapidly until $W \approx 1$. If the experiments had been run for much longer times, larger values of W_a would have been observed as W increases when the mixed layer deepens.

As shown in §§3.1 and 3.2, the development with time of the mixed-layer density is a good indicator of the upwelling process. Figure 15 (*a*) shows a plot of mixed-layer density as functions of time at the six profile stations used in experiment 29 ($W = 12$). Even at this large value of W, large horizontal density gradients in the mixed layer are created by upwelling. The pattern in this case is somewhat different from that

Experiment	W	$\langle\Delta\rho\rangle g/\rho$ cm s^{-2}	$\langle h\rangle$ cm	u_*^2 cm^2 s^{-2}	W_a	$(h_1/H)_{obs}$	$(h_1/H)_{calc}$
29	12.0	1.6	14.0	0.2	1.0	0.33	0.35
28	4.0	1.6	14.0	0.9	1.0	0.56	0.50
30	2.5	2.0	10.0	0.7	0.8	0.50	0.59
32	1.7	2.5	10.5	0.9	0.9	0.60	0.66

TABLE 3. Average W at steady state in a linearly-stratified fluid
All symbols defined in text.

shown in figure 8 as in this case the density gradient decays with time, at least until approximately T_1, at which time the gradient appears to stabilize.

Figure 15(*b*), a plot of mixed-layer density in experiment 32, also shows the exponential decay of the horizontal density gradient seen in figure 15(*a*), but in addition shows somewhat more clearly, that after this decay, the gradient becomes constant while the actual mixed-layer density continues to decrease. Thus if the stratification is linear, large horizontal gradients are created initially by upwelling. These weaken with time, eventually reaching an equilibrium point where they then evolve in the same fashion as is observed for two-layer flows; i.e. the upwelling buoyancy flux balances the longitudinal buoyancy flux, causing the mixed-layer density to change uniformly along the tank.

3.4. *Upwelling at low Wedderburn number, $W < 1$*

When $W < 1$, tilting of the interface in a two-layered fluid is severe enough for total upwelling to occur. In lakes, this means that hypolimnetic water flows up to the surface, replenishing fluid that is advected downwind in the surface layer. In these experiments, it means that fluid from the upper layer reaches the belt at or near $x = 0$, the 'upwind' end of the tank. While the theory (SI) predicts rapid, shear-driven deepening of the mixed layer, the present experiments show another, different mixing mechanism. Where the interface intersects the belt, a front develops in which there is intense mixing due to advectively-created density inversions; the effect of this local mixing is then spread throughout the rest of the mixed layer by shearflow dispersion. This mixing mode starts as soon as the interface intersects the belt, and mixes out all but a small fraction of the initial density difference in the mixed layer at a time

$$T_m = \frac{0.03\,L^2}{h_2\,u_*}, \tag{8}$$

in agreement with the shearflow dispersion theory given in SI.

To illustrate the development over time of the density field when $W < 1$, profiles (figure 16(*a–d*)) and contours (figure 17(*a–d*)) from experiment 24 ($W = 0.45$) are presented. In this case, the contours are made up using monotonic versions of the profiles, so that none of the density inversions present in the profiles are present in the contours. The contours do however represent the mean state of the density field, as the density inversions tended to be short-lived.

The initial profile can be seen in figure 16(*a*); the interface occupies approximately 20 % of the total depth (i.e. 2 cm). The first contour, figure 17(*a*), taken at $t = 0.35\,T_1$ shows the large-scale tilting of the interface. Somewhat unexpectedly, the centre region is tilted more severely than either of the two ends. The outer edge of the interface has begun to intersect the belt, and the $10\,\sigma_t$ contour has been stripped

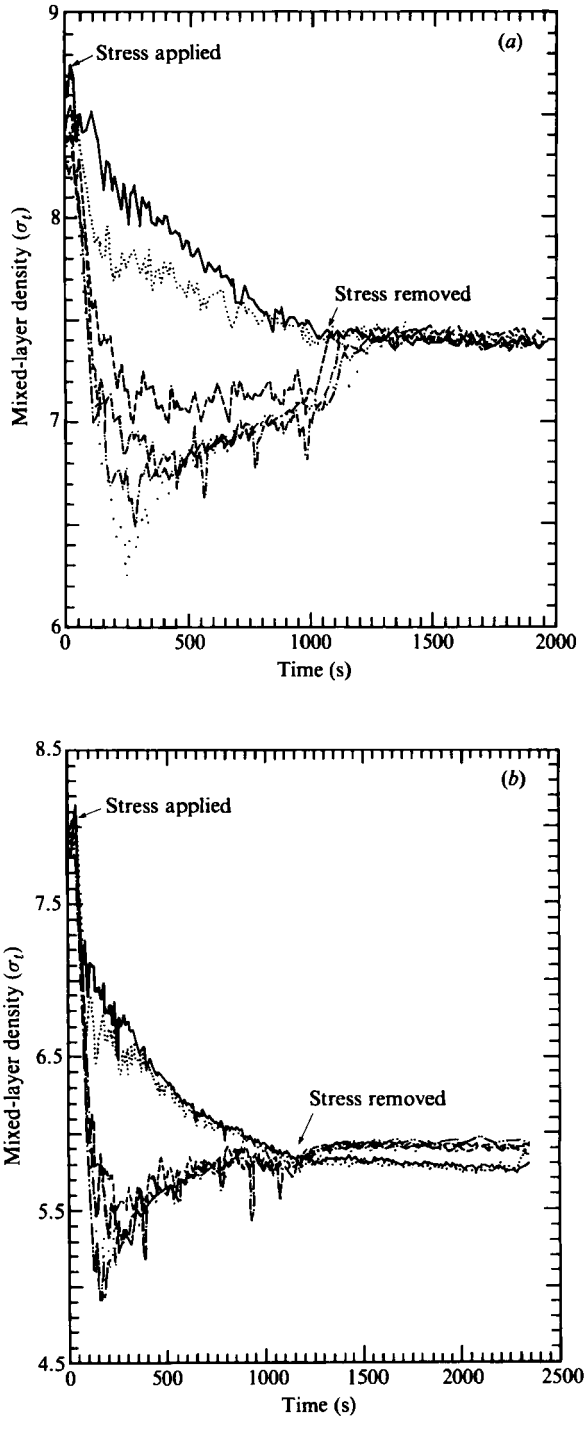

FIGURE 15. (*a*) Mixed-layer density as functions of time during experiment 29 at $\cdots$, $x = 0.10\,L$; —··—, $x = 0.20\,L$; —·—, $x = 0.30\,L$; – – –, $x = 0.40\,L$; · · · · · ·, $x = 0.60\,L$; and ——, $x = 0.80\,L$. (*b*) Mixed-layer density as functions of time at various locations along the axis of the tank during experiment 32. The symbols have the same meaning as those in (*a*).

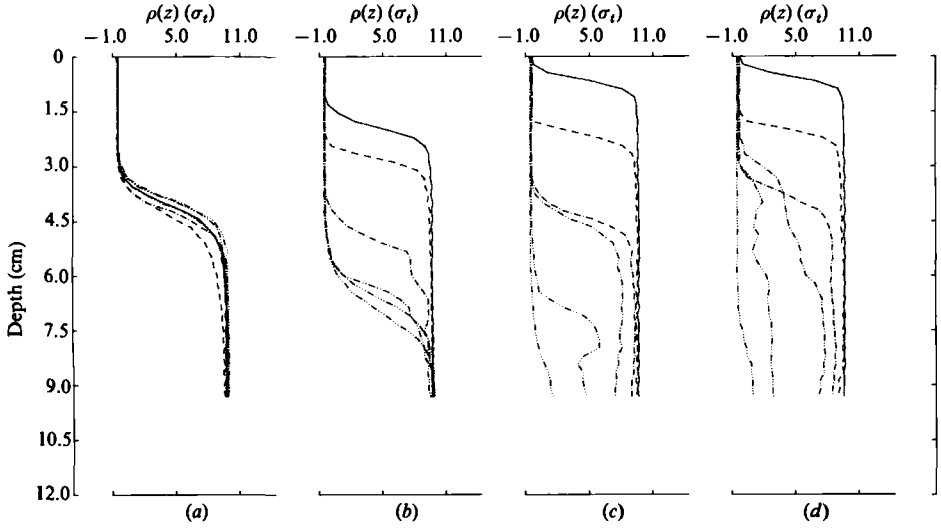

FIGURE 16. Vertical profiles of density during the initial phase of experiment 24. The profiles were taken at the same locations as those shown in figure 14(*a–d*). These sets of profiles were taken at (*a*) $t = 0.00\,T_1$; (*b*) $t = 0.27\,T_1$; (*c*) $t = 0.53\,T_1$; and (*d*) $t = 0.70\,T_1$.

away from the interface. By $t = 0.5\,T_1$, (figure 17*b*), the entire interface intersects the belt between $x \approx 50$ and 100 cm and begins to disintegrate. Figure 17(*c*) shows that by $t = 0.7\,T_1$ a sharp front has developed near $x = 100$ cm. As the experiment proceeds, the front diffuses and more and more of the isopycnals in the interface are stripped away; by $t = 1.0\,T_1$ (figure 17*d*), density differences in the mixed layer are comparable to those existing between the two layers.

The quasi-state flow pattern in low-W experiments was similar to that observed in higher W experiments. Figure 18 shows a sketch of the flow pattern which created the inversions seen in the lower part of the water column in figure 16(*c* and *d*). The upwind flow advected heavier fluid upwind as the downwind flow advected lighter fluid downwind. A shadowgraph of the upwelling region (taken in experiment 18, $W = 0.4$), figure 19, shows the intense mixing that took place as these inversions collapsed and new inversions were created. This type of vertical mixing appears to be that described by Blanton (1973) as edge leakage. The similarity between figure 19 and figure 6, the corresponding picture for $W > 1$, should be noted.

The exact form of stratification did not affect the response when W was sufficiently small. The single low W experiment, experiment 15 ($W = 0.4$), conducted with a linear stratification gave results indistinguishable from those obtained using two-layer stratifications at similar values of W.

The present experiments do not show evidence of Kelvin–Helmholtz billowing. Several factors may have contributed to this. Consider experiment 24: using the results of SI, the maximum velocity difference would be calculated to have been 11.2 cm s^{-1}; according to Sherman, Imberger & Corcos (1978), $\delta_s = 0.3(\Delta U)^2/g' = 0.3(11.2)^2/10 = 3.8$ cm. The initial thickness was 2 cm so that billowing should have been expected to double the interface thickness. This value must be reduced on two accounts. First, the nearest measuring station to $x = \frac{1}{2}L$ was at $x = 0.4\,L$; this means a reduction of 20% in the maximum shear relative to the maximum shear at $x = \frac{1}{2}L$ (Spigel 1978). Secondly, the shear must be corrected for the effect of the steady circulation since it is set up in a time $O(h_2/u_*)$, and thus is set up

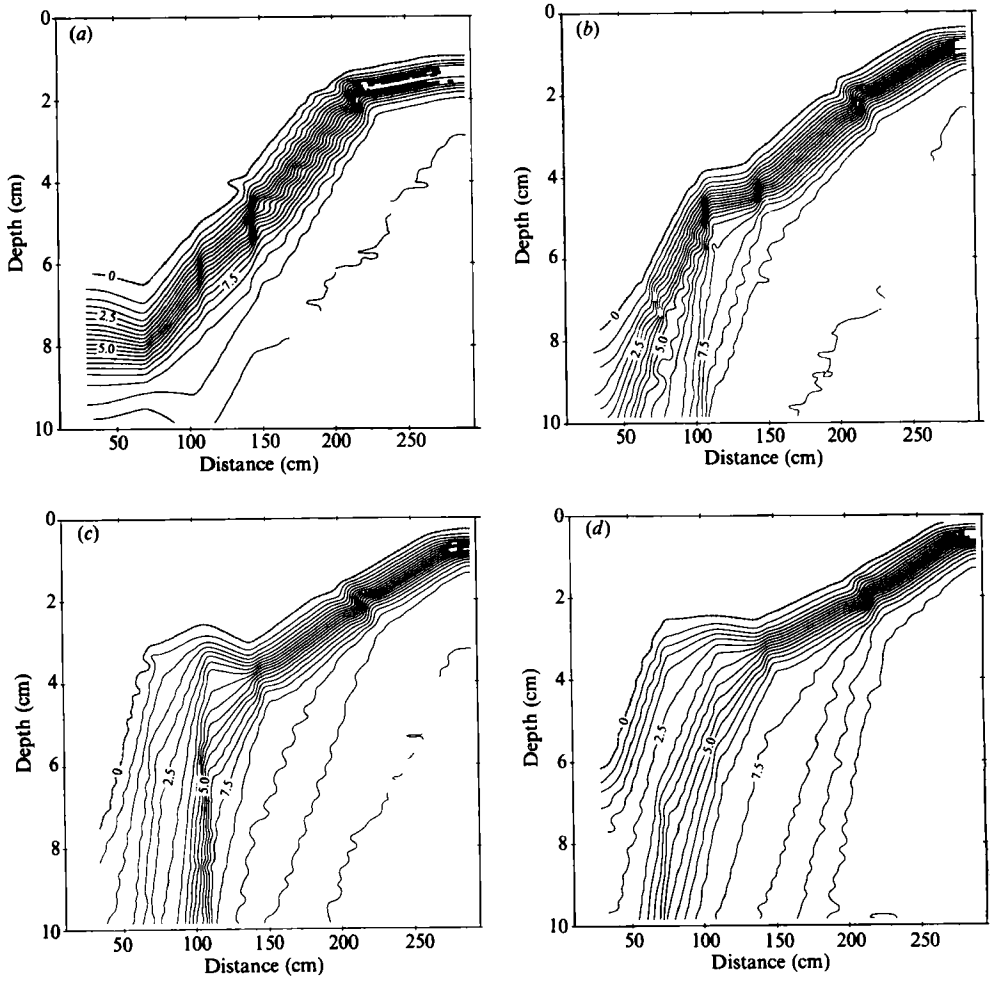

FIGURE 17. Contour plots of the density field during the initial phase of experiment 24. The contours show conditions existing at (*a*) $t = 0.35\,T_1$; (*b*) $t = 0.53\,T_1$; (*c*) $t = 0.70\,T_1$; (*d*) $t = 1.05\,T_1$.

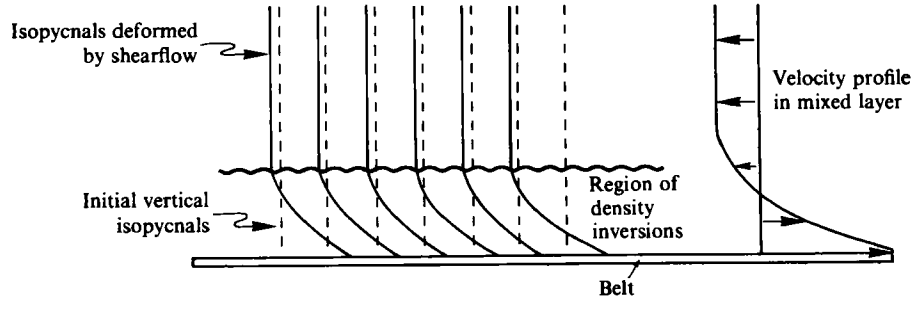

FIGURE 18. Sketch of velocity and density profiles in the upwelling region when $W < 1$. The shear flow in the horizontally-stratified mixed layer tilts the near-vertical isopycnals, creating density inversions which are unstable and lead to mixing.

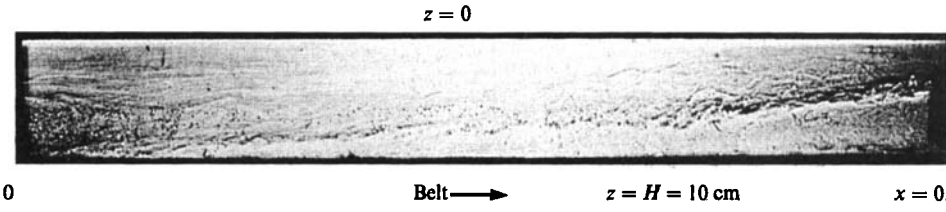

FIGURE 19. Shadowgraph of the upwelling region in experiment 18 ($W = 0.4$, 2 layers).

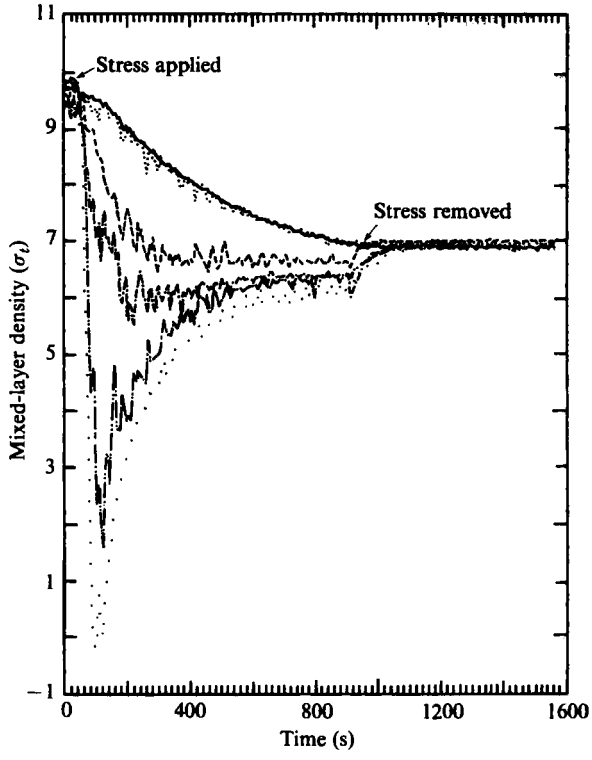

FIGURE 20. Mixed-layer density as a function of time during experiment 24. The symbols have the same meaning as those in figure 15(*a*) and (*b*).

before the seiche-induced currents reach their peak. As it is in opposition to the seiche-induced flow, the steady circulation, $U_s \sim 2u_*$ (Kit, Berent & Vadja 1980; Keulegan & Brame 1960), reduces the interfacial shear, ΔU, and thus also reduces shear production of TKE and the size of Kelvin–Helmholtz billows (or suppresses them entirely). The net effect is to make these shear-driven mixing processes somewhat weaker than suggested by SI. Using the estimates given above, the exact reduction in ΔU is seen to depend on W, L/h_1, and H/h_2. In order that ΔU be 90% of the value assumed by SI, it is necessary that

$$W \leqslant 6.3 \times 10^{-4} \left(\frac{L}{h_1}\right)\left(\frac{H}{h_2}\right). \tag{9}$$

According to (9), quite large values of the aspect ratio L/h_1 are required for the scaling of SI to be valid. For example, if $W = 1$, and $H = 2h_1$, L/h_1 must be at least 800. This large value of L/h_1 would most likely be found only in quite shallow layers

such as the shallow ($L/h_1 \sim 2000$) diurnal mixed layer studied in Imberger (1985). The good agreement of the SI theory and Imberger's (1985) observations is not surprising as the large values of L/h_1 reported by Imberger were observed in conjunction with quite small values of $W(O(10^{-2}))$; given the observed aspect ratios, the observed values of W were well below that required by (9) to ensure that the shear can be calculated without taking into account the reduction due to the steady circulation.

Figure 20 plots the density in the mixed layer at each of the profiling stations as a function of time throughout experiment 24 and shows that the mixed-layer density plummets near $x = 0$ as upwelling proceeds. Near $x = 280$ cm, there is initially very little change in the mixed-layer density. Once upwelling is complete (at $t \approx 0.7\,T_1$), with an e-folding time of 250 s, the density field exponentially approaches a uniform state. Using (10), the formula of SI 95% completion of horizontal mixing, gives $T_m = 300$ s. The experimental data shows $T_m \approx 1000$ s. While SI assumed that as a result of shear stability and upwelling (acting in an unspecified fashion), the density would vary linearly in the x-direction and would not vary at all in the z-direction, in the present case the initial horizontal density gradient was more concentrated than SI assumed; this would tend to make T_m larger than the value given by (9). Further, upwelling continued after mixing had begun, maintaining the density on the 'windward' side of the front; this too would tend to increase T_m. Given these two important differences between the experiments and what is assumed by the theory, the discrepancy between (9) and the observations is not large.

4. Mixing mechanisms

4.1. *Longitudinal dispersion and horizontal mixing*

The experimental time series of mixed-layer density, samples of which can be found in figures 8, 15(a, b) and 20, all show the presence of horizontal density gradients in the mixed layer. When $W < 1$, this gradient reaches a maximum value at $t \approx 0.5\,T_1$, and decreases thereafter. There is little vertical stratification, so that changes in mixed-layer density must be due to the horizontal buoyancy flux.

When $W > 1$, the horizontal density gradient does not vary with time; thus, the mixed-layer density decreases uniformly with time. This observation can be interpreted in two ways: firstly, horizontal variations in vertical mixing, due to substantial variations in the mixed-layer Richardson number (defined in (4)), are smoothed out by longitudinal dispersion, allowing mixed-layer deepening near $x = L$ to keep up with deepening near $x = 0$. Alternately, a balance could exist between longitudinal dispersion which tends to eliminate any horizontal density gradients, and upwelling which tends to create those gradients. The mixed-layer density gradient would reach an equilibrium state in which any increase in upwelling would be suppressed by increased mixing while any increase in mixing and hence reduction in the gradient would be met by an increased upwelling flow. In the present experiments, the upwelling region (near $x = 0$) would act as a source of lighter fluid which would be 'diffused' (dispersed) downwind. This model is pursued in detail in the Appendix.

Suppose that all of the observed change in mixed-layer density can be attributed to upwelling and longitudinal dispersion. This is certainly the case for the $W < 1$ experiments, and is a useful hypothesis for $W > 1$ experiments. Making this assumption, the longitudinal dispersion coefficient ϵ_x can be estimated as follows:

away from the upwelling region itself, it can be assumed that the change in mixed-layer density is due entirely to dispersion so that (SI):

$$\partial_t \rho_m = \epsilon_x \partial^2_{xx} \rho_m, \tag{10}$$

where ρ_m is the density of the mixed layer at some point x and at time t. When written in finite-difference form, (10) gives an expression for ϵ_x, viz.

$$\epsilon_x = \frac{(\rho_i(t+\Delta t) - \rho_i(t))\,(x_i - x_j)^2}{\langle \rho_i - \rho_j \rangle\,(\Delta t)}, \tag{11}$$

where ρ_i is the density at x_i, ρ_j is the density at x_j, and $\langle \rho_i - \rho_j \rangle$ is the mean density difference between x_i and x_j during the time t and $t+\Delta t$. The results of this calculation are shown in table 4 for a number of experiments, representing two-layered and linear stratifications, and experiments with $W < 1$ and $W > 1$. Although there is substantial scatter, due both to the simple form of mixing assumed, and to a lack of horizontal resolution, the calculated dispersion coefficients appear to be independent of W and the type of stratification (no trend can be discerned), giving a mean value of $\epsilon_x \approx 3 h_2 u_*$. This agrees reasonably well with the theoretical value of 6.3 suggested by SI. The constant of proportionality appearing in the expression for ϵ_x is discussed further in the Appendix.

The timescale for horizontal mixing is not significantly affected by the difference between measured and theoretical values of ϵ_x, especially as T_m is dependent on the x distribution of density in the mixed layer. Hence, the value suggested by SI for T_m is adequate for estimating the time required to reach the equilibrium gradient.

4.2. *Mixed-layer deepening when $W > 1$*

The rate of change of mixed-layer density can also be used to calculate the effective rate of mixed-layer deepening when $W > 1$. Since the thickness of the interface did not change as a result of mixing in the experiments, conservation of buoyancy (assuming a linear equation of state for salt water) can be adequately approximated by writing

$$\frac{\mathrm{d}}{\mathrm{d}t}(\Delta \rho h_2) = 0, \tag{12}$$

implying that

$$\frac{\mathrm{d}h_2}{\mathrm{d}t} = -\frac{h_2\,\mathrm{d}\Delta\rho/\mathrm{d}t}{\Delta\rho}. \tag{13}$$

All of the experiments were run for periods sufficiently short that initial values of h_2 and $\Delta\rho$ can be used in (13) to calculate the average, effective rate of mixed-layer deepening, $\mathrm{d}h_2/\mathrm{d}t$, from the observed rate of change of mixed-layer density (equivalent to $\mathrm{d}\Delta\rho/\mathrm{d}t$ since the density of the upper layer fluid does not change). The results of this calculation are shown in figure 21 where $\mathrm{d}h_2/\mathrm{d}t$, normalized by u_*, is plotted, for two-layer experiments, as a function of Ri. Within the scatter of the experimental data, the results of the present study agree with those of Kranenburg (1985) which were obtained in a much larger flume. These data can be approximately represented by the formula

$$\frac{\mathrm{d}h_2/\mathrm{d}t}{u_*} = 0.07\, Ri^{-1}. \tag{14}$$

Equation (14) gives entrainment rates somewhat lower than suggested by Wu (1973) who found a constant of proportionality of 0.23 rather than 0.07.

The measurements of the density field presented in §3 suggest that a plausible

Experiment	W	Stratification	$(\rho_i(t+\Delta t)-\rho_i(t))(\Delta t)^{-1}$ kg m^{-3} s^{-1}	$\langle\rho_i-\rho_j\rangle(\Delta x)^{-2}$ kg m^{-5}	$\epsilon_x(u_* h_2)^{-1}$
8	3.9	2L	4.0×10^{-4}	1.6×10^{-1}	2.8
20	1.7	2L	1.3×10^{-3}	6.1×10^{-1}	4.5
21	1.7	2L	9.0×10^{-4}	5.0×10^{-1}	4.0
22	1.7	2L	9.0×10^{-4}	2.0×10^{-1}	4.1
24	0.4	2L	5.0×10^{-3}	4.0	1.0
				2.0	2.5
28	4.0	L	1.2×10^{-4}	5.0×10^{-1}	2.2
29	12.0	L	4.0×10^{-4}	2.0	1.5
32	1.7	L	1.0×10^{-3}	2.0	2.8

TABLE 4. Observed dispersion coefficients

For experiments with linear stratifications W in the table is calculated using total depth; 2L = two-layer stratification and L = linear stratification; In experiment 24 the first row using $x_1 = 2.10$ m and $x_2 = 1.40$ m while the second row was calculated using $x_2 = 0.70$ m.

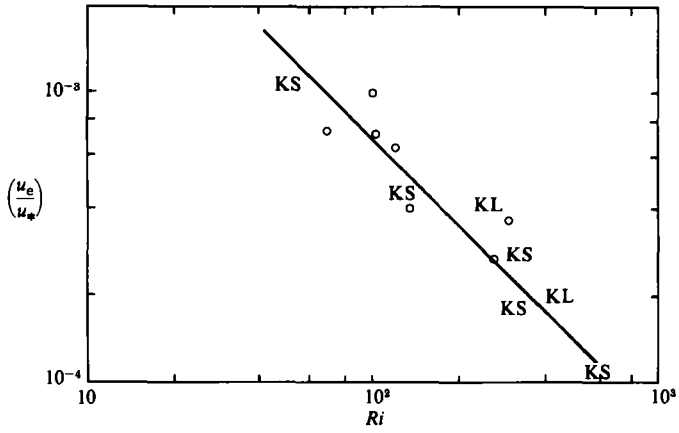

FIGURE 21. Rate of mixed-layer deepening $u_e = dh_2/dt$, normalized by u_*, plotted as function of the mixed-layer Richardson number, $Ri = g'h_2/u_*^2$ for two-layered experiments. ○, this study (2L); KS, KL, Kranenburg (1985); ——, $0.07\,Ri^{-1} = u_e/u_*$.

model for mixed-layer deepening would be one in which fluid at the edge of the mixed layer is dragged along the interface until, as the interface diverges and partially intersects the stressed surface (the belt in the experiments and the free surface in the field), it is brought to the surface and is subsequently mixed downwind by longitudinal dispersion in the mixed layer. Such a model is presented in the Appendix.

5. Discussion and conclusions

The experimental results presented in the lst three sections demonstrate the importance of both the Wedderburn number W, and the density distribution in determining the dynamic response. While the theory of SI replaces the original parameters Ri and A with a single parameter, W, the experiments show that A must be retained as an independent parameter if it is not greater than approximately 800. This is because, at smaller values of A, the unsteady, baroclinic shear is reduced by

the steady mixed-layer circulation. Furthermore, A also determines the relative sizes of the timescale for longitudinal dispersion and for the baroclinic response. However, it appears that the pair of parameters, (W, A), is more useful for describing the flow than is the pair of parameters (Ri, A).

While W can be used to delineate qualitatively different regimes of dynamic response and the extent of upwelling, the actual response depends on the distribution of the stratification. In the present experiments there are considerable differences between experiments with $\delta/H \approx 0.2$ (those referred to as two-layer experiments in the body of the text) and experiments in which $\delta/H \approx 1.0$ (those referred to as linearly-stratified experiments in the body of the text). In general, if the stratification is continuous, and if the Wedderburn number based on the overall density contrast and total depth, or a large part of the total depth (e.g. $\frac{1}{2}$ as in the present experiments), > 1, a new $\Delta\rho$, less than the total $\Delta\rho$, can always be chosen so as to make $W_m \approx 1$. This behaviour was best exhibited by those experiments performed using linear statifications. The subscript m is used because this intrinsic Wedderburn number is, in effect, a mixed-layer Wedderburn number, as opposed to the bulk Wedderburn number which is defined using bulk properties and which embodies first-mode dynamics. This is analogous to the case of inertial selective withdrawal where if the Froude number determined by bulk parameters is less than the critical Froude number, a new Froude number defined using withdrawal layer thickness will be approximately equal to the critical value (Turner 1973).

If W, calculated using bulk properties, < 1, the classical two-layer representation of upwelling is valid; if in addition, $W \ll 1$, the one-dimensional analysis presented in SI should be valid. If $W < 1$, but still $O(1)$, the mixing process is highly two-dimensional; for the aspect ratios used in the present study, mixing is dominated by longitudinal dispersion of horizontal density variations created directly by upwelling, and by overturning in the upwelling region itself.

An interesting case arises for a two-layer fluid in which initially $h_1/H \ll 1$ and W is $\ll 1$. At first the layer will deepen one-dimensionally, and so W will increase. If W becomes $O(1)$ before the wind stops or before the mixed layer hits the bottom of the reservoir, the subsequent response should be similar to the case in which $W = O(1)$ initially, meaning that mixing must eventually become two-dimensional.

The observations suggest that the response at $W > 1$ is much more complex than the two-layer model predicts. Although the interface sharpens, at least at the downwind end of the tank, due to application of the stress, this sharpening is temporary and local; at the upwind end of the tank the interface is diffuse. When the stress is removed, the interface rethickens at the downwind end and resharpens at the upwind end. Density distributions similar to those seen in figures 9(*d*) and 15(*d*) have been observed in lakes by Wedderburn (1912), Mortimer (1952), and, more recently Imberger (1985) and in those numerical simulations of the response of stratified lakes to wind stresses reported by Thompson & Imberger (1980) and by Church & Thompson (1982).

These distortions of the interface have little to do with mixing, but instead, represent the dynamic adjustment of the density field to the applied stress. Distortion of the interface can, in principle, be accounted for by considering a three-layer model of the stratification (as in Csanady 1982, or Monismith 1985). However, as shown in Monismith (1986), the observations of the set-up of the divergent interface are not entirely consistent with the results of the linear, normal-mode analysis. It seems likely that a numerical solution may be required to determine the exact mechanism of interfacial distortion. Furthermore such simula-

tions would be of considerable use in determining the effects the geometry of the endwalls at $x = 0$ and $x = L$ has on the core flow (the horizontal flow away from the up- and down-welling regions) since the laboratory box is a far cry from the complex basin shapes found in nature. However, barring the possibility that changing the end-wall geometry effects major differences in the core flow, it should be concluded that when a stratified lake is subjected to wind stresses, and if $W > 1$, those isopycnals closest to the free surface will be affected most.

Upwelling appears to play a major role in determining the rate of mixed-layer deepening. For $W > 1$, the rate of change of mixed-layer density was uniform along the length of the tank; this observation could plausibly be described as the result of a combination of upwelling and longitudinal dispersion. A simple model of this process, one in which the upwelling buoyancy flux is specified at $x = 0$ and is assumed to be switched on at $t = 0$ and to be constant thereafter, shows that the density gradient in the mixed layer evolves on a timescale of (L^2/ϵ_x). What observations are available are in quite good agreement with the theory. However, while the present experiments and theory do not conclusively prove that entrainment across the interface proper is not important, they do show that if results from experiments such as these are to be used in the formulation of models of mixed-layer deepening in lakes and reservoirs, proper account must be taken of the effects of upwelling.

The experiments described in this paper would not have been attempted were it not for the multi-faceted support generously provided to the author by Dr C. van Ingen. The author thanks Professor J. Imberger for reading several drafts of this manuscript and for engaging in numerous discussions concerning the model of mixed-layer deepening by upwelling given in the Appendix. The author also wishes to thank R. Denton, D. Ford, G. Lawrence, R. Spigel, R. Street and S. G. Schladow. Mr E. White and Mr P. Dale of the Hydraulics Laboratory of the University of California built the experimental apparatus.

This research was supported by the University of California Water Resources Center as part of project UCAL-WRC-W 592. Additional funds for computing were provided by the Centre for Environmental Fluid Dynamics at the University of Western Australia. This manuscript was prepared while the author was employed by the Centre for Water Research at the University of Western Australia.

Lastly, the author expresses his gratitude to the late Professor H. Fischer for his supervision of this work.

Appendix: A model for deepening due to upwelling when $W > 1$

By J. Imberger† and S. Monismith

The results of the investigation described in the main part of this paper, and the measurements reported in Keulegan & Brame (1960) and Kranenburg (1985) can be used to formulate a simple model of the effect of upwelling on mixed-layer deepening. All of the experimental data support the following conclusions concerning upwelling and mixed-layer deepening in two-layered fluids (two layers separated by an interface having finite thickness):

(*a*) The interface tilts and opens up at the upwind end over a period of time approximately equal to the internal seiche period T_1 (given by (3)). The data suggest that the isopycnals are almost horizontal at the bottom of the interface, but slope

† Centre for Water Research, University of Western Australia, Nedlands, WA 6009, Australia.

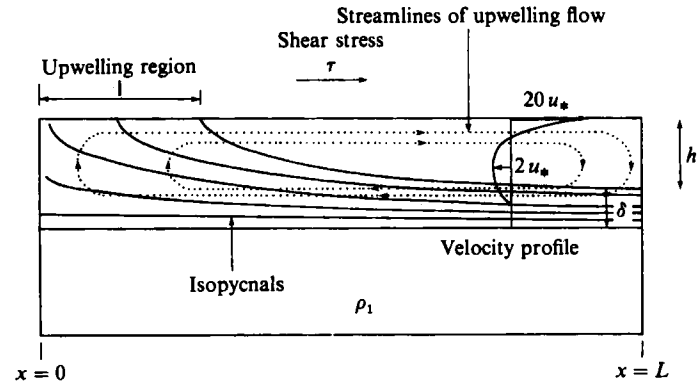

FIGURE 22. Definition sketch for model of mixed-layer deepening due to upwelling.

upward considerably at the top of the interface. A weak, horizontal density gradient is established in the mixed layer by a combination of upwelling and horizontal variations in turbulent entrainment.

(*b*) The velocity profile in the surface layer is such that the velocity of the stressed surface is approximately $20u_*$ and about $2u_*$ at the interface. This observation differs from the assumption made by SI who assumed that the recirculating flow in the mixed layer could be neglected for $W > 1$. As pointed out in §3.4, neglect of the steady velocity field for times less than T_1 is only permissible when the mixed-layer aspect ratio (L/h_1) is large (e.g. $O(10^3)$).

(*c*) The upwelling region itself is confined to the upwind end of the basin. The density in the surface layer increases with time; for $t \gg T_m$, the shearflow dispersion timescale, $\partial_t \rho$ is nearly independent of x.

(*d*) The entrainment law which best fits the experimental data is

$$\frac{dh_1}{dt} = C_1 u_* Ri^{-1}, \tag{A 1}$$

where C_1 is a constant between 0.07 (Kranenburg 1985 and this study) and 0.23 (Wu 1973).

These conclusions permit the construction of a simple model of upwelling and mixed-layer deepening for reservoirs when $W > 1$. A definition sketch for this model is shown in figure 22. Upon application of the shear stress the interface tilts and spreads; since tilting and spreading are comparable,

$$\delta \approx \zeta \approx \frac{Lu_*^2}{B_0}, \tag{A 2}$$

where δ is as shown in figure 22, $B_0 = \{(\rho_1 - \rho_0) g h_1\}/\rho_0 = g_0' h_1$ is the initial value of the mixed-layer buoyancy, h_1 is the initial mixed-layer depth, and ζ is the mean interfacial deflection (as given by (2)).

Interfacial fluid is dragged to the surface in the upwelling region by the steady flow in the mixed layer. It then is mixed downwind by shearflow dispersion. A net entrainment law can be constructed using this combination of upwelling and mixing. The horizontal buoyancy flux in the interface is

$$\delta u_* g_a' \sim L_a' \left(\frac{dh}{dt}\right), \tag{A 3}$$

where, if ρ_a is the average density in the mixed layer, $g'_a = g(\rho_1 - \rho_a)/\rho_0$, and h is the mixed-layer depth at any time. It follows that

$$\frac{\mathrm{d}h}{\mathrm{d}t} = \frac{\delta u_*}{L}. \tag{A 4}$$

If δ satisfies (A 2) substituting (A 2) into (A 4) produces a result consistent with (A 1). Thus, the Ri^{-1} entrainment law can be arrived at without invoking interfacial entrainment; instead, it is the consequence of upwelling.

The buoyancy flux (given by (A 3)) introduced into the main part of the mixed layer at the upwind end by upwelling is mixed downwind by shear flow dispersion. Thus, the perturbation buoyancy field in the mixed layer $g'_m(x,t) = (\rho(x,0,t) - \rho_0)\, g/\rho_0$ satisfies the diffusion equation (Fischer *et al.* 1979):

$$\partial_t g'_m = \epsilon_x \partial^2_{xx} g'_m, \tag{A 6}$$

where

$$\epsilon_x = C_2 h u_* \tag{A 7}$$

is the effective diffusion coefficient. The coefficient C_2 depends on the shape of the velocity profile and on the distribution and magnitude of the vertical diffusivity (ϵ_z). SI estimated that $C_2 \approx 6$, which is the value Elder (1959) derived for the log profile characteristic of two-dimensional open channel flow. However, C_2 will remain unspecified for the moment.

The width of the end region, 1, is approximately h_1, as in this region vertical and horizontal velocities are comparable. In effect, the upwelling region is just that region where the upwind flow in the mixed layer and interface is turned around and redirected downwind (as in the case of cavity flow studied by Cormack, Leal & Imberger 1974). An upper bound on 1 can be obtained by noting that in the upwelling region, the flow is locally unstable because the upwelled fluid is forced to flow over lighter fluid. Hence, 1 is also the distance travelled by a particle as it falls a distance $\frac{1}{3}h_1$, the distance from the surface to the point of zero horizontal velocity, under the influence of a buoyancy force which depends on x and the buoyancy gradient in the upwelling region. In terms of the upwelling buoyancy flux, β, the length l can be shown to be (assuming an average surface velocity of $4u_*$):

$$l \approx u_* (\tfrac{1}{3}C_2)^{\frac{1}{3}} h_1^{\frac{2}{3}} \beta^{-\frac{1}{3}}. \tag{A 8}$$

Using (A 3),

$$\beta = (C_1 l u_*^3)/h_1^2; \tag{A 9}$$

thus,

$$l \approx \left(\frac{C_2}{3C_1}\right)^{\frac{1}{3}} h_1^{\frac{4}{3}} L^{-\frac{1}{3}}. \tag{A 10}$$

Using typical values of $C_1 = 0.07$ and $C_2 = 6$, l is seen to be approximately $4h_1(h_1/L)^{\frac{1}{3}}$, i.e. proportional to h_1 with a weak dependence on (h_1/L).

A simple quantitative model of how upwelling leads to mixed-layer deepening can be formulated by assuming that initially the mixed layer is homogeneous and by modelling the effect of upwelling as an impulsively-started, and later constant buoyancy flux of strength β at $x = 0$. Thus, the temporal and spatial variations of g'_m can be found by solving (A 6) subject to the following boundary and initial conditions:

$$\partial_x g'_m(0,t) = (\beta/\epsilon_x)\, H(t); \tag{A 11a}$$

$$\partial_x g'_m(L,t) = 0; \tag{A 11b}$$

and

$$g'_m(x,0) = 0. \tag{A 11c}$$

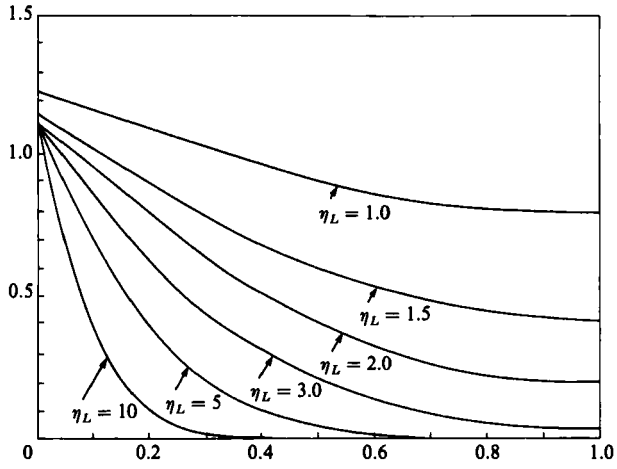

FIGURE 23. Curves of the solution (A 12) for $\Gamma = g'_{\rm m}(x,t)/(\beta t^{\frac{1}{2}}\epsilon_x^{-\frac{1}{2}})$ as functions of x at different values of $\eta_L = L/(\epsilon_x t)^{\frac{1}{2}}$.

The required solution can be found in Carslaw & Jaeger (1978) as

$$g'_{\rm m}(x,t) = 2\beta(t/\epsilon_x)^{\frac{1}{2}} \sum_{n=0}^{\infty} [\text{ierfc}\{(2nL+L-x)\,(2(\epsilon_x t)^{\frac{1}{2}})^{-1}\} + \text{ierfc}\{(2nL+x)\,(2(\epsilon_x t)^{\frac{1}{2}})^{-1}\}], \tag{A 12}$$

where $\text{ierfc} = \{\exp(-x^2)/\pi^{\frac{1}{2}}\} - x\,\text{erfc}(x)$, and erfc is the complementary error function. Equation (A 12) is plotted in figure 23 in terms of the quantity $\Gamma = g'_{\rm m}(x,t)\,\epsilon_x^{\frac{1}{2}}\beta^{-1}t^{-\frac{1}{2}}$ for different values of $\eta_L = L/(\epsilon_x t)^{\frac{1}{2}}$. When comparing experimental data with this solution, an allowance must be made for the fact that horizontal density gradients are created during the initial period of set-up by upwelling and by shear-driven entrainment, i.e. $g'_{\rm m}(x,0) = f(x)$. This can be done by adjusting the time origin either through addition or subtraction of an offset. Ideally, this offset should be much less than the characteristic timescale of the dispersion process:

$$T_0 = \frac{L^2}{\epsilon_x}. \tag{A 13}$$

In addition, since β depends on h, it is not really constant throughout the experiment. The solution will only be valid for times somewhat less than

$$T_{\rm v} = \frac{h_1 Ri}{C_1 u_*}, \tag{A 14}$$

the time required for the mixed-layer depth to double. The ratio of T_0 to $T_{\rm v}$ is

$$T_{\rm r} = \frac{T_0}{T_{\rm v}} = \left(\frac{C_1}{C_2}\right)\left(\frac{L}{h_1}\right) W^{-1}; \tag{A 15}$$

if $(L/h_1) \approx (C_2/C_1)$, $T_{\rm r}$ is $O(1)$, and the solution given in (A 12) is only valid for $t < T_0$.

From the solution plotted in figure 23 it can be seen that the effect of the upwelling flux is not felt at $x = L$ until $t \approx 0.11\,T_0$, at which time $g'_{\rm m}(L) \approx 0.04\,g'_{\rm m}(0)$. The total density difference in the mixed layer reaches a maximum at $t \approx 0.25\,T_0$, remains

constant until $t \approx T_0$, and then begins to drop as the mixed layer 'heats up'. The solution for $g'_m(0,t)$ can be shown to be

$$g'_m(0,t) = 2\beta t^{\frac{1}{2}} \epsilon_x^{-\frac{1}{2}} \pi^{\frac{1}{2}}, \tag{A 16}$$

for times less than $0.44\,T_0$. Finally, $g'_m(0,t)$ will equal g'_0 when

$$t = T_f = \tfrac{1}{4}\pi \left(\frac{C_2}{C_1^2}\right) W^2 \left(\frac{h}{u_*}\right). \tag{A 17}$$

If $T_f > 0.44\,T_0$, the factor appearing in (A 17) will not be $\frac{1}{4}\pi$.

The theory presented above can be compared with measurements reported in the body of the paper, with measurements taken by Keulegan & Brame (1960), and with measurements taken by Kranenburg (1985); in all three cases, measurements of the mixed-layer density at different locations and different times are available. To make the comparison, values of C_1 and C_2, must first be chosen. In terms of the chosen values of these two constants, the observed value of Γ can be found to be:

$$\Gamma = \left(\left(\frac{C_2}{C_1}\right)\left(\frac{h_1}{L}\right) W \eta_L\right)\left(\frac{g'_m}{g'_0}\right), \tag{A 18}$$

where g'_m is now calculated using measured values of ρ. The most convenient means of presenting the data is in terms of Γ/η_L at different values of $\xi = x/L$ plotted as functions of $\tau = t/T_0$.

Figure 24 presents data from experiment 8 of this study converted according to (A 18), using $C_1 = 0.07$ (that value determined experimentally) and $C_2 = 6$. The densities measured at $\xi = 0.08$ and 0.87 asymptotically approach their theoretical values as diffusion smears away the initial effects of upwelling. It should be noted that the particular value of C_2 chosen is twice that which was estimated in §4.1. However, this value of C_2 gives a better fit of the data to the theory at both locations than either $C_2 = 3$ or 10. The value of ϵ_x derived by obtaining the best possible fit of the data to the theoretical curves should be considered equal in accuracy to the value of ϵ_x computed using a finite difference form of (A 6).

Figure 25 shows the data from three experiments reported in Keulegan & Brame (1960), from two experiments reported in Kranenburg (1985) and, from experiment 8 of the present study. In reducing these data, the following operations have been performed:

(i) C_1 was first chosen to be 0.07 and, for all except experiment 8, C_2 was chosen to be 10;

(ii) the resulting 'raw' curves were plotted;

(iii) so as to best-fit the data to the theoretical curves, the dimensionless time was offset by an amount $\Delta\tau$ and C_1 was altered.

The last step was interactive and was performed first for the data from the ξ position, say ξ_1, closest to $\xi = 0$. Once a satisfactory fit was obtained for ξ_1, the data at a second position, $\xi_2 > 0.5$, was then reduced using the final values of C_1 and $\Delta\tau$. From trial and error, it became apparent that for each experiment analysed, a best set of values of ($\Delta\tau$, C_1, and C_2) existed which appeared to minimize the differences between theory and measurements for both values of ξ. In all cases, reasonable values of all three parameters were obtained: the time offsets were always less than $0.04\,T_0$, and the entrainment coefficient C_1 was between 0.05 and 0.133, well within the range reported in the literature and cited above. The difference between values of C_2 chosen for the belt-driven flow and the wind-driven flows may reflect differences in the

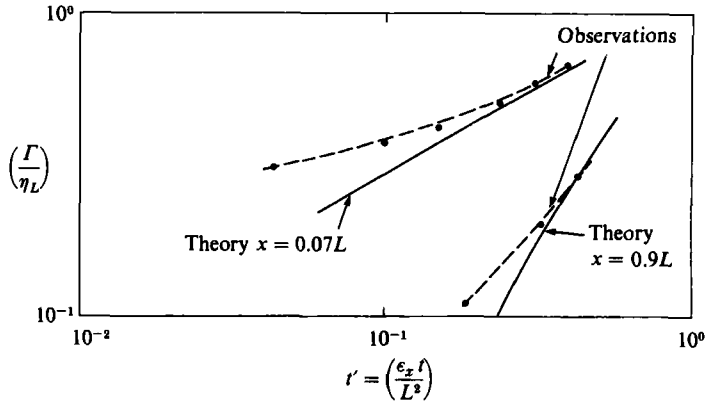

FIGURE 24. Plot of values of (Γ/η_L) calculated from densities at $\xi = 0.08$ and $\xi = 0.87$ measured during experiment 8 ($W = 3.9$) of this study. The theoretical curves are shown as the solid lines.

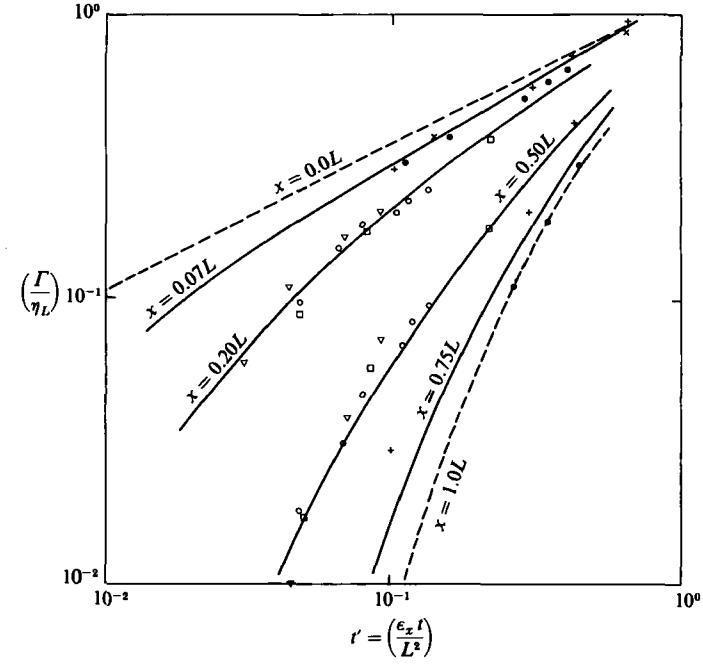

FIGURE 25. Plot of values of (Γ/η_L) calculated from densities measured with correction for the initial conditions and adjusted for a best-fit of data at two values of ξ. The solid lines are the theoretical solution while the symbols represent: ●, experiment 8 this study, $W = 3.9$, $\Delta\tau' = 0.060$, $C_1 = 0.07$, $C_2 = 6$; △, Keulegan & Brame (1960) $W = 3.0$, $\Delta\tau' = 0.015$, $C_1 = 0.11$, $C_2 = 10$; ○, Keulegan & Brame (1960) $W = 2.4$, $\Delta\tau' = 0.025$, $C_1 = 0.11$, $C_2 = 10$; □, Keulegan & Brame (1960) $W = 1.5$, $\Delta\tau' = 0.030$, $C_1 = 0.05$, $C_2 = 10$; +, Kranenburg (1985) $W = 3.7$, $\Delta\tau' = -0.015$, $C_1 = 0.11$, $C_2 = 10$; ×, Kranenburg (1985) $W = 2.3$, $\Delta\tau' = +0.010$, $C_1 = 0.11$, $C_2 = 10$.

structure of those flow, especially in the way the shear stress and surface velocity vary with x.

In summary, the comparison between theory and observations presented in figures 24 and 25, is quite good. Unfortunately, no experimental results are available to describe the final phase of mixed-layer deepening, that which occurs after the surface density at $x \approx 0$ reaches ρ_1. If such observations were available, the mechanism of mixed-layer deepening by upwelling might be further clarified.

REFERENCES

BLANTON, J. O. 1973 Vertical entrainment into the epilimnia of stratified lakes. *Limnol. Oceanogr.* **18** (5), 697–701.

CARSLAW, H. S. & JAEGER, J. C. 1978 *Conduction of Heat in Solids*, 3rd edn. Oxford University Press.

CHURCH, J. A. & THOMPSON, R. O. R. Y. 1982 Cloud-in-cell and finite difference models for a stratified lake. In *Numerical Solutions of Partial Differential Equations* (ed. J. Noye). North Holland.

CORMACK, D. E., LEAL, L. G. & IMBERGER, J. 1974 Natural convection in a shallow cavity with differentially heated end walls. Part 1. Asymptotic theory. *J. Fluid Mech.* **65**, 209–230.

CSANADY, G. T. 1982 On the structure of transient upwelling events. *J. Phys. Oceanogr.* **12** (1), 84–96.

ELDER, J. W. 1959 The dispersion of marked fluid in turbulent shear flow. *J. Fluid Mech.* **5**, 544–560.

FERNANDO, H. J. S. & LONG, R. R. 1983 The growth of a grid-generated mixed layer in a two fluid system. *J. Fluid Mech.* **133**, 377–395.

FISCHER, H. B., LIST, E. J., KOH, R. C. Y., IMBERGER, J. & BROOKS, N. H. 1979 *Mixing in Inland and Coastal Waters*. Academic.

FITZGERALD, L. M. & MANSFIELD, W. W. 1965 The response of closed channels to wind stress. *Austral. J. Phys.* **18**, 219–226.

HEAPS, N. S. & RAMSBOTTOM, A. E. 1966 Wind effects on water in a narrow two-layered lake. *Phil. Trans. R. Soc. Lond.* A **259**, 391–430.

HELLSTRÖM, B. 1941 Wind effects on lakes and rivers. *Ingren Vetensk. Akad. Handl.* 158 pp.

IMBERGER, J. 1985 The diurnal mixed layer. *Limnol. Oceanogr.* **30**, 737–771.

KEULEGAN, G. 1951 Wind tides in small closed channels. *J. Res. Nat. Bur. Stand.* **47**, 358–381.

KEULEGAN, G. & BRAME, V. 1960 Fourteenth Progress report on model laws for density currents: mixing effects of wind-induced waves. *Nat. Bur. Stand. Rep.* NBS-6638, 35 pp.

KIT, E., BERENT, E. & VADJA, M. 1980 Vertical mixing induced by wind and a rotating screen in a stratified fluid in a channel. *J. Hyd. Res.* **18** (1), 35–57.

KOSEFF, J. R. & STREET, R. L. 1985 Circulation structure and mixing processes in a stratified lid-driven cavity flow. *J. Hydraul. Div. ASCE* **111** (HY2), 334–354.

KRANENBURG, C. 1984 Wind-induced entrainment in a stably stratified fluid. *J. Fluid Mech.* **145**, 253–273.

KRANENBURG, C. 1985 Mixed-layer deepening in lakes after wind set-up. *J. Hydraul. Div. ASCE* **111** (HY9), 1279–1297.

KRAUS, E. B. & TURNER, J. S. 1967 A one-dimensional model of the seasonal thermocline. II. The general theory and its consequences. *Tellus* **14**, 98–105.

LIGHTHILL, M. J. 1969 Dynamic response of the Indian Ocean to the Southwest Monsoon. *Phil. Trans. R. Soc. Lond* A **265**, 45–92.

LINDEN, P. F. 1979 Mixing in stratified fluids. *Geophys. Astrophys. Fluid Dyn.* **13**, 3–23.

MONISMITH, S. G. 1983 The dynamic response of stratified reservoirs to surface shear stress. *Rep. No.* UCB/Hel-83-05, Hydraulic Engineering Laboratory, University of California, Berkeley, California.

MONISMITH, S. G. 1985 Wind induced motions in stratified lakes and their effect on mixed-layer shear. *Limnol. Oceanogr.* **30**, 771–786.

MONISMITH, S. G. 1986 The modal response of reservoirs to wind stress. (submitted to *J. Hydraul. Div. ASCE*).

MORTIMER, C. H. 1952 Water movements in lakes during summer stratification. Evidence from the distribution of temperature in Windmere. *Phil. Trans. R. Soc. Lond.* B **236**, 255–404.

POLLARD, R. T., RHINES, P. B. & THOMPSON, R. O. R. Y. 1973 The deepening of the wind mixed layer. *Geophys. Fluid Dyn.* **3**, 381–404.

SCHLICHTING, H. 1975 *Boundary Layer Theory*. McGraw-Hill.

SHERMAN, F. S., IMBERGER, J. & CORCOS, G. M. 1978 Turbulence and mixing in stably stratified waters. *Ann. Rev. Fluid Mech.* **10**, 267–288.

SPIGEL, R. H. 1978 Wind mixing in lakes. Ph.D. thesis, University of California at Berkeley.

SPIGEL, R. H. & IMBERGER, J. 1980 The classification of mixed layer dynamics in lakes of small to medium size. *J. Phys. Oceanogr.* **10** (7), 1104–1121.

SPIGEL, R. H., IMBERGER, J. & RAYNER, K. N. 1986 A model for billowing and deepening of the diurnal mixed layer. *Limnol. Oceanogr.* **31**, 533–566.

STEFAN, H. & FORD, D. E. 1975 Temperature dynamics of dimictic lakes. *J. Hydraul. Div. ASCE* **101** (HY2), 334–354.

THOMPSON, R. O. R. Y. & IMBERGER, J. 1980 Response of a numerical model of a stratified lake to wind stress. *Proc. 2nd Intl Symp. Stratified Flows, Trondheim, June 1980* **1**, 562–570.

THORPE, S. A. 1977 Turbulence and mixing in a Scottish Loch. *Phil. Trans. R. Soc. Lond.* A **286**, 125–181.

TURNER, J. S. 1973 *Buoyancy Effects in Fluids.* Cambridge University Press.

WEDDERBURN, E. M. 1912 Temperature observations in Loch Earn with a further contribution to the hydrodynamical theory of temperature seiches. *Trans. R. Soc. Edinb.* **48**, 629–695.

WU, J. 1973 Wind-induced entrainment across a stable density interface. *J. Fluid Mech.* **61**, 257–287.

WU, J. 1977 A note on the slope of a density interface between two stably stratified fluids under wind. *J. Fluid Mech.* **81**, 335–339.